SyNPL: Synthetic Notch pluripotent cell lines to monitor and manipulate cell interactions *in vitro* and *in vivo*.

Running title: Engineering cell interactions

Mattias Malaguti[1,‡], Rosa Portero Migueles[1], Jennifer Annoh[1], Daina Sadurska[1,2], Guillaume Blin[1], Sally Lowell[1,‡]

1. Centre for Regenerative Medicine, Institute for Stem Cell Research, School of Biological Sciences, University of Edinburgh, 5 Little France Drive, Edinburgh EH16 4UU, UK
2. Current address: Sir William Dunn School of Pathology, University of Oxford, Oxford, United Kingdom

‡ Authors for correspondence: mattias.malaguti@ed.ac.uk sally.lowell@ed.ac.uk

Keywords: Cell interaction; SynNotch; pluripotent stem cells; cell engineering, patterning.

ABSTRACT

Cell-cell interactions govern differentiation and cell competition in pluripotent cells during early development, but the investigation of such processes is hindered by a lack of efficient analysis tools. Here we introduce SyNPL: clonal pluripotent stem cell lines which employ optimised Synthetic Notch (SynNotch) technology to report cell-cell interactions between engineered "sender" and "receiver" cells in cultured pluripotent cells and chimaeric mouse embryos. A modular design makes it straightforward to adapt the system for programming differentiation decisions non-cell-autonomously in receiver cells in response to direct contact with sender cells. We demonstrate the utility of this system by enforcing neuronal differentiation at the boundary between two cell populations. In summary, we provide a new tool which could be used to identify cell interactions and to profile changes in gene or protein expression that result from direct cell-cell contact with defined cell populations in culture and in early embryos, and which can be adapted to generate synthetic patterning of cell fate decisions.

INTRODUCTION

During embryogenesis, pluripotent cells undergo a series of cell fate decisions that are controlled by interactions between epiblast cells, their early differentiated derivatives, and the surrounding extraembryonic tissues (Arnold and Robertson, 2009; Nowotschin and Hadjantonakis, 2010; Rossant and Tam, 2009). The transcriptional changes that accompany exit from pluripotency and differentiation into specific cell types have been extensively characterised, and the long-range signals that control these changes are now well understood (De Los Angeles et al., 2015; Kinoshita and Smith, 2018; Pera and Tam, 2010; Posfai et al., 2021; Tam and Loebel, 2007). Less is known about how early developmental decisions are influenced by direct interactions of cells with their neighbours. It is well established that cell-cell interactions play a key role in development (Dias et al., 2014; Gurdon, 1987; Johnson and Ziomek, 1983; Schultz, 1985), but until recently there has been a paucity of molecular and technological tools available to study these processes in detail in relevant settings (Nishida-Aoki and Gujral, 2019; Yang et al., 2021).

Quantitative image analysis can be used to identify and infer the effect of neighbours on the properties of cells of interest in fixed samples (Blin et al., 2018; Fischer et al., 2020; Forsyth et al., 2021; Toth et al., 2018). We have recently developed a software suite for automated neighbour identification during live imaging (Blin et al., 2019), which provides researchers with a further dimension to study the effects on cell-cell interactions on cell fate decisions. Whilst live image analysis provides high-resolution visual information, this approach is labour-intensive and only leads to neighbour identification *a posteriori*.

The nascent field of Synthetic Developmental Biology (Davies, 2017; Ebrahimkhani and Ebisuya, 2019; Ho and Morsut, 2021; Santorelli et al., 2019; Schlissel and Li, 2020) seeks to understand the mechanisms of patterning and cell differentiation through the engineering of genetic circuits (Cachat et al., 2016; Matsuda et al., 2015; Sekine et al., 2018). By re-engineering the Notch/Delta signalling cascade, Lim and colleagues generated a synthetic circuit capable of reporting and manipulating cell-cell interactions in real time (Morsut et al., 2016). In this system, a "sender" cell presenting an extracellular membrane-bound antigen of interest is recognised by a "receiver" cell expressing a chimaeric Synthetic Notch (SynNotch) receptor, composed of an extracellular antigen-recognition domain, the Notch1 core transmembrane domain containing proteolytic cleavage sites, and an intracellular synthetic effector domain (Fig. 1). Thanks to the modularity of the SynNotch circuitry, it is therefore possible to interrogate and manipulate the effects of interactions between cell types of interest.

SynNotch technology has been used for monitoring cell-cell interactions, generating synthetic patterns, generating synthetic morphogen gradients, inducing contact-mediated gene editing, and generating custom antigen receptor T-cells (Cho et al., 2018; Choe et al., 2021; He et al., 2017; Huang et al., 2020; Roybal et al., 2016; Sgodda et al., 2020; Toda et al., 2018; Toda et al., 2020; Wang et al., 2021). SynNotch technology has been established in *Drosophila* (He et al., 2017) as well as in immortalised cell lines and differentiated cell types, but its potential in the study of mammalian developmental events remains largely untapped.

Mouse embryonic stem cells (ESCs) can be differentiated into any cell type of interest *in vitro*, can give rise to chimaeric embryos and can be used to establish transgenic mouse lines (Bradley et al., 1984; Evans and Kaufman, 1981; Martin, 1981). Adapting the SynNotch system for use in mouse ESCs would therefore permit monitoring and manipulation of cell-cell interactions in a developmental context both *in vivo* and *in vitro*. The original system designed by (Morsut et al., 2016) used lentiviral transduction of immortalised and primary cell lines, where transgene expression was driven from the retroviral SFFV promoter. Lentiviral transduction can lead to multiple copy transgene integration in mouse ESCs (Pfeifer et al., 2002), and the SFFV promoter is prone to silencing in mouse pluripotent cells and their derivatives (Herbst et al., 2012; Pfaff et al., 2013; Wu et al., 2011), making this system suboptimal for mouse ESCs.

In this study, we made a number of adaptations to the original SynNotch system (Morsut et al., 2016) in order to establish clonal modular SynNotch pluripotent cell lines (SyNPL). We characterised the properties of this SyNPL system by monitoring interactions between eGFP-expressing sender cells and mCherry-inducible receiver cells *in vitro*, then showed that this system can report interactions between neighbouring cells *in vivo* in chimaeric mouse embryos, that it can be used for synthetic patterning, and that its flexible and modular design can be exploited to conveniently manipulate cell-cell interactions and drive contact-mediated synthetic cell fate engineering.

RESULTS

Design of SyNPL ESCs

We set out to adapt the SynNotch system, which was previously established through viral transduction of immortalised mouse L929 fibroblasts and K562 erythroleukaemic cells (Morsut et al., 2016), for use in mouse ESCs. In this system, sender cells are labelled with membrane-tethered extracellular eGFP (Fig. 1A). Receiver cells constitutively express a SynNotch receptor composed of an anti-GFP nanobody (LaG17) (Fridy et al., 2014), the mouse Notch1 minimal transmembrane core (Uniprot: Q01705, residues 1427-1752), and a tetracycline transactivator (tTA) (Gossen and Bujard, 1992), and contain a tetracycline response element (TRE) promoter capable of driving *mCherry* expression in response to tTA binding (Fig. 1B). Interaction of eGFP on sender cells with the anti-GFP nanobody on receiver cells leads to cleavage of the Notch1 core, releasing the tTA which can translocate to the nucleus, bind to the TRE promoter and drive *mCherry* expression (Fig. 1C). In addition, we constitutively labelled receiver cells with a tagBFP-3xNLS construct (Fig. 1B,C) to conveniently identify them by fluorescence microscopy and flow cytometry even in the absence of a contact-dependent mCherry signal.

Our aims when adapting the SynNotch system were to generate ESC lines with low cell-cell variability, robust and sustained transgene expression, and a modular design to allow convenient transgene exchange. In order to avoid cell-cell variability we elected to generate clonal cell ESC lines with stable genomic integration of the SynNotch system components, delivering transgenes by electroporation rather than lentiviral transduction to reduce the risk of multi-copy integration (Boggs et al., 1986; Charrier et al., 2011; Pfeifer et al., 2002; Smithies et al., 1985). We sought to ensure uniform levels of transgene expression by screening clonal lines and/or targeting transgenes to specific genomic locations, and by replacing the silencing-prone SFFV retroviral promoter used by (Morsut et al., 2016) with CAG (Niwa et al., 1991) or mouse *Pgk1* (McBurney et al., 1991) promoters, which have been extensively characterised in mouse ESCs (Chen et al., 2011; Hong et al., 2007). Finally, we set out to introduce modularity to our system by generating a “landing platform” master cell line to allow recombination-mediated cassette exchange (RMCE) of transgenes of interest.

Generation of extracellular membrane-tethered eGFP-expressing sender ESCs

We first generated clonal sender cell lines expressing membrane-tethered extracellular eGFP. The CAG and mouse *Pgk1* promoters are both silencing-resistant promoters commonly used to drive ubiquitous transgene expression in ESCs. We set out to determine which of these promoters can generate viable sender cells with strong and uniform expression of membrane eGFP. We also wished to explore whether eGFP molecules with HA and Myc protein tags can retain “sender” function in pluripotent cells.

We electroporated mouse ESCs with four sender constructs, containing either CAG or mouse *Pgk1* promoters driving expression of either untagged or HA- and Myc-tagged eGFP fused to a membrane-tethering domain (Fig. 2A-D). We isolated and expanded 64 clonal lines derived from stable genomic integration of the four constructs, and screened them by flow cytometry, analysing median eGFP intensity (Fig. 2E,F), percentage of eGFP-positive cells (Fig. 2G,H) and eGFP distribution (Figs. S1, S2). Both CAG and *Pgk1* promoters are capable of driving high uniform expression of eGFP, and as expected, there is considerable variability in eGFP expression between clonal lines.

We selected one untagged eGFP sender clone (CmGP1) and one HA- and Myc-tagged eGFP sender clone (CHmGMP19), exhibiting high, uniform and similar levels eGFP expression (Fig. 2I) for further analysis. For both clones, the pattern of eGFP expression appeared to be consistent with membrane localisation, and, in the case of CHmGMP19, eGFP co-localised with Myc (Fig. 2J,K).

129 **Generation of a safe harbour site landing pad master ESC line**

130 To facilitate convenient and repeated modification of the genome, we generated a clonal ESC line
131 carrying a "landing pad" targeted to the *Rosa26* locus, a safe harbour site in the mouse genome
132 (Friedrich and Soriano, 1991). This landing pad contains a splice acceptor, the *Neo* (G418/geneticin
133 resistance) gene, and a CAG promoter driving expression of *mKate2-3xNLS*, which encodes a red
134 fluorescent protein with no evident phenotypic effect in mouse embryos (Malaguti et al., 2013;
135 Shcherbo et al., 2009). This entire cassette is flanked by two *attP50* sites, which allows for ϕC31
136 integrase-mediated recombination with cassettes flanked by two *attB53* sites (Huang et al., 2009;
137 Tosti et al., 2018) (Fig. S3A). After confirming insertion at the correct genomic locus (Fig. S3B), we
138 verified that all cells express high and uniform levels of mKate2-3xNLS (Fig. S3C,D). We named this cell
139 line EM35.

140 **An "all-in-one" design fails to generate fully functional mCherry inducible receiver cells**

141 We first set out to investigate whether it would be possible to target all transcriptional units required
142 for receiver cell activity to the *Rosa26* landing pad in EM35 ESCs, and whether this would lead to the
143 generation of functional receiver ESCs. The design and characterisation of the resulting cell lines is
144 explained in detail in Supplementary Methods and Figs. S4-S9. Briefly, we found that mCherry could,
145 as expected, be induced by subpopulations of tagBFP-positive receiver cells in response to interaction
146 with eGFP-positive sender cells, but that this particular receiver cell design was hampered by variable
147 levels of tagBFP, variable inducibility of mCherry, and low levels of the SynNotch receptor. We
148 conclude that the SynNotch receptor construct and *TRE-mCherry* cassette can function as expected in
149 ESCs, but that further modifications to the design are required to obtain a reliable contact-reporting
150 system.

151 **A multi-step design produces fully functional mCherry-inducible receiver ESCs**

152 We hypothesised that two independent events may be affecting mCherry inducibility during our initial
153 attempts to generate "all-in-one-locus" receiver cells (Figs. S4-S9). Firstly, we speculated that *mCherry*
154 and *tagBFP* transgenes may have been lost from the genome due to mitotic recombination (Stern,
155 1936) or due to errors in replication at similar DNA sequences in close proximity (*Pgk1* promoters,
156 *bGHpA* signals). Secondly, we suspected that the expression levels of the SynNotch receptor were not
157 sufficient for efficient mCherry induction (Fig, S9).

158 We planned to circumvent the issue of potential loss of DNA by physically separating the three
159 transcriptional units through random genomic integration of the SynNotch receptor cassette and of
160 the *tagBFP-3xNLS* cassette, and by removing identical DNA sequences. To attempt to increase levels
161 of SynNotch receptor and to obtain uniform levels of tagBFP-3xNLS, we added an internal ribosome
162 entry site (IRES) followed by *Ble* (zeocin resistance gene) downstream of the SynNotch receptor
163 sequence, and an IRES followed by *Hph* (hygromycin B resistance gene) downstream of the *tagBFP-*
164 *3xNLS* sequence (Fig. 3A).

165 In order to generate these cells, we first randomly integrated the SynNotch receptor construct into
166 the genome of EM35 landing pad ESCs (Fig. S10A). We screened 87 clones for Myc expression, and
167 selected two clones (35SRZ9, 35SRZ86) with high, uniform Myc expression (Fig. S10B). The levels of
168 Myc in these clones were higher than those observed in receiver cells generated with an all-in-one
169 design (clones SNCB+4 and SNCB-6) and higher than those observed in Myc-tagged sender cells
170 (CHmGMP19) (Fig. S10C). We then randomly integrated the *tagBFP-3xNLS* transgene into the genome
171 of these two clones (Fig. S10D). We screened a total of 36 clones and selected one for each parental

172 line with high, uniform expression of tagBFP-3xNLS (PSNB-A clone 10, PSNB-B clone 3) (Fig. S10E,F).
173 We renamed these lines PSNB (Parental SynNotch tagBFP) clones A and B respectively.

174 Next, we performed RMCE at the *Rosa26* landing pad in PSNB cells to replace the *mKate2* transgene
175 with one of three constructs: the *TRE-mCherry* cassette present in the SCNB construct, a *tetO-mCherry*
176 cassette with more tTA binding sequences elements in the inducible promoter (to test whether this
177 led to improved mCherry induction), or an empty vector cassette to generate tagBFP-positive mKate2-
178 and mCherry-negative control cell lines (Fig. S11A). We verified that integration of the empty vector
179 cassette led to loss of mKate2 expression, and used these control cell lines to confirm that tagBFP
180 signal was able to unambiguously identify receiver cells (Figs. 3B,C, S11B).

181 We then set out to test whether the new receiver cell lines containing inducible mCherry cassettes
182 expressed mCherry in response to co-culture with sender cells. We screened 27 clones for tagBFP and
183 mCherry expression by culturing them in the presence or absence of sender cells for 24 hours (Fig.
184 S11C-F). We observed that all genetically identical clones behaved very similarly, suggesting we were
185 not experiencing silencing or loss of DNA. Clones containing the larger *tetO-mCherry* cassette
186 exhibited high levels of mCherry leakiness in the absence of sender cells. Co-culture with sender cells
187 led to significant mCherry induction, but the distributions in the presence and absence of sender cells
188 overlapped significantly (Fig. S11D,F). Clones containing the smaller *TRE-mCherry* cassette exhibited
189 mCherry leakiness in the absence of sender cells, however co-culture with sender cells led to an
190 increase in mCherry expression to levels which displayed minimal overlap with those seen in cells
191 cultured in the absence of sender cells (Fig. S11C,E). We selected three clones with minimal leakiness
192 and high inducibility for downstream analysis (PSNBA-TRE1, PSNBB-TRE10, PSNBB-TRE9). We renamed
193 these cells STC (for SynNotch-TRE-mCherry) clones A1, B1 and B2 respectively. We verified that these
194 receiver lines could induce mCherry following cell-cell interaction with sender cells by co-culturing
195 sender and receiver cells together for 24 hours. We observed specific induction of mCherry by tagBFP-
196 positive receiver cells in contact with eGFP-positive sender cells (Fig. 3D). We used flow cytometry to
197 confirm that mCherry is robustly induced in the majority of tagBFP-positive receiver cells following co-
198 culture with 9-fold excess of CmGP1 sender cells at confluence (Fig 3B,C,E,F).

199 These observations suggest that physical separation of the three transcriptional units in the genome
200 of receiver cells, coupled to the use of internal ribosome entry sites and selectable markers within the
201 units, can lead to the generation of receiver ESC lines which exhibit clear and specific induction of
202 mCherry upon interaction with eGFP-expressing sender cells.

203 **Extracellular membrane-tethered eGFP is required for contact-mediated transgene induction in**
204 **receiver cells**

205 It would be useful to make use of existing GFP fluorescent reporter ESCs (for example, cell-state
206 reporters or signalling reporters) to act as sender cells, in order to test how particular cell states may
207 influence direct neighbours. However, many such cell lines make use of non-membrane-tethered GFP,
208 which is unlikely to interact with the anti-GFP nanobody on STC receiver cells. We therefore wished
209 to test whether membrane tethering of eGFP to the extracellular space was absolutely necessary for
210 effective neighbour-labelling.

211 We profiled mCherry levels in STC receiver cells by flow cytometry following 24 hours of co-culture
212 with "sender" cells carrying different transgenes (Fig. 3E-H). We cultured STC receiver cells alone (Fig.
213 3E), in the presence of CmGP1 sender cells (Fig. 3F), in the presence of a control cell line expressing
214 untagged intracellular eGFP (E14GIP1) (Fig. 3G), or in the presence of CmGP1 sender cells containing
215 an extra untagged intracellular eGFP transgene (CmGP1GH1) (Fig. 3H). We found that E14GIP1 cells,

216 which do not express membrane-tethered eGFP, did not induce mCherry above baseline levels in in
217 co-cultured STC receiver cells (Fig. 3E-G). Furthermore, we observed that mCherry is induced to similar
218 levels following co-culture with either CmGP1 or CmGP1GH1 sender cells (Fig. 3F,H), suggesting that
219 the additional untagged eGFP transgene in CmGP1GH1 cells does not interfere with mCherry induction
220 by the extracellular eGFP transgene. We conclude that cells containing intracellular GFP would not be
221 capable of functioning as sender cells unless supplemented with extracellular membrane tethered
222 eGFP.

223 **Increasing sender:receiver cell ratios leads to increased transgene induction in receiver cells**

224 We next set out to establish how differing sender:receiver cell ratios could affect the efficiency of
225 neighbour-labelling. We co-cultured STC receiver cells with different proportions of sender cells for 24
226 hours (Fig. S12). We observed that as few as 20% of sender cells were sufficient to induce mCherry in
227 approximately half of STC receiver cells, and that 90% sender cells could induce mCherry in over 90%
228 of STC receiver cells (Fig. S12A,B). mCherry fluorescence follows a bimodal distribution in receiver cells
229 exposed to "non-saturating" numbers of sender cells, and a unimodal distribution in receiver cells
230 exposed to "saturating" numbers of sender cells (Fig. S12C-H). This suggests that STC receiver cells
231 which have come into contact with sender cells can uniformly induce high levels of mCherry
232 expression, as observed by immunofluorescence when co-culturing cells at a 9:1 sender:receiver cell
233 ratio (Fig. S12I-K).

234 **HA- and Myc-tags on eGFP do not affect sender cell function**

235 An epitope tag fused to eGFP could be helpful for unequivocally identifying and isolating sender cells,
236 but carries the risk of interfering with sender function. Having generated sender cells with HA- and
237 Myc-tagged (CHmGMP19) and untagged (CmGP1) eGFP molecules, we sought to understand whether
238 tagged and untagged eGFP differed in their ability to induce transgene expression in receiver cells. We
239 therefore compared the ability of each sender line to induce mCherry expression in the previously
240 described experiment, where we cultured STC receiver cells with CmGP1 or CHmGMP19 sender cells
241 at varying sender:receiver cell ratios (Fig. S12). Both CmGP1 and CHmGMP19 sender cell lines can
242 drive mCherry induction to similar extents (Fig. S12A-H), suggesting that the LaG17 nanobody on the
243 SynNotch receptor can recognise both untagged and HA- and Myc-tagged eGFP, and that these tags
244 do not compromise sender function.

245 **Kinetics of contact-dependent transgene induction in receiver cells**

246 We next set out to ask how long sender cells need to be in contact with receiver cells in order to trigger
247 mCherry labelling, and to characterise the kinetics of mCherry induction. We filmed STC receiver cells
248 co-cultured with CmGP1GH1 sender cells for 24 hours (Fig. 4A, Movie 1). We first observed mCherry
249 induction 5-6 hours after initial sender-receiver contact (Fig. 4A, yellow arrowheads), with a rapid
250 increase in mCherry levels until the 16-hour timepoint, and a slower increase thereafter. We observed
251 STC receiver cells which did not make contact with sender cells and remained mCherry-negative (Fig.
252 4A, magenta arrowheads), and an STC receiver cell that made contact with a sender cell 2 hours before
253 the cells were fixed at the 24-hour timepoint for immunofluorescence, and which remained mCherry-
254 negative (Fig. 4A, cyan arrowheads).

255 We then quantified the kinetics of mCherry induction. We co-cultured 10% STC receiver cells with 90%
256 CmGP1 sender cells, and analysed mCherry expression by flow cytometry over the course of 72 hours
257 (Fig. 4B). mCherry is first induced at low levels at the 5-hour timepoint, and its expression keeps
258 increasing until the 48-hour timepoint (Figs. 4C,D, S13A,B).

259 mCherry protein maturation will introduce a time-lag between initiation of mCherry transcription and
260 the detection of mCherry fluorescence. For example, when analysing further timelapse experiments
261 (Fig. 4E, Movie 2), we noticed an example of an STC receiver cell which remained in contact with a
262 sender cell for 8 hours, lost contact for 12 hours following a cell division, but kept increasing its levels
263 of mCherry in the meantime (Fig. 4E, white arrowheads). Relying on direct detection of mCherry (Fig
264 4A-D) is therefore likely to overestimate the minimum duration of cell contact required for mCherry
265 induction.

266 We designed an experimental strategy to overcome this problem. We co-cultured 10% STC receiver
267 cells with 90% CmGP1 sender cells for various time points between 0 and 24 hours, then added
268 doxycycline to the culture medium for a further 16 hours (Fig. 4F). Doxycycline prevents tTA from
269 binding to *TRE* sequences (Gossen and Bujard, 1992), hence we expect doxycycline administration to
270 halt *mCherry* transcription in receiver cells while still allowing time for mCherry protein to mature.
271 This means that any mCherry signal observed after doxycycline administration should be ascribable to
272 cell-contact-dependent transcription that took place during the initial period of co-culture in
273 doxycycline-free medium. In this experimental setting, we observed low but detectable induction of
274 mCherry when cells had experienced only 2 hours of doxycycline-free co-culture (Figs. 4G,H, S13C,D).

275 These data collectively suggest that 2 hours of sender-receiver contact may be sufficient for induction
276 of low levels of mCherry, and that mCherry levels will keep increasing in receiver cells for a period of
277 time following the loss of sender-receiver contact. This neighbour-labelling system can therefore
278 identify receiver cells that have had relatively brief interactions with sender cells or which have
279 recently lost contact with sender cells.

280 **Kinetics of contact-dependent mCherry perdurance in receiver cells**

281 We next sought to establish how long mCherry signal persisted following loss of tTA-mediated
282 *mCherry* transcription. We co-cultured 10% STC receiver cells with 90% CmGP1GH1 cells for 24 hours,
283 then added doxycycline to the culture medium (to block the activity of tTA and halt mCherry
284 transcription) and filmed the cells over 48 hours (Fig. S14A,B, Movies 3,4). We observed little change
285 in mCherry fluorescence for the initial 10-12 hours, then a gradual decrease in signal until its
286 extinguishment around 38-40 hours after doxycycline addition (Fig. S14A,B). In order to quantify this
287 process, we co-cultured 10% STC receiver cells with 90% CmGP1 sender cells for 24 hours, then added
288 doxycycline to the culture medium and analysed mCherry fluorescence by flow cytometry at various
289 timepoints (Fig. S14C). No reduction of mCherry signal was observed for the initial 8 hours following
290 doxycycline administration, with median mCherry expression decreasing by approximately half by 16
291 hours, and mCherry signal returning to background levels within 48 hours (Fig. S14D-F).

292 Taken together, these results suggest that induction of mCherry occurs more rapidly than loss of
293 mCherry signal, presumably due to the high stability of this fluorescent protein, further confirming the
294 utility of this system for identifying recent as well as current cell-cell interactions.

295 **The SyNPL SynNotch cell-cell interaction reporter is functional in early mouse embryos**

296 Having comprehensively characterised the SynNotch system in clonal mouse ESC lines, we set out to
297 test whether the system could also function *in vivo* in early mouse embryos. We aggregated wild-type
298 morulae with CmGP1GH1 sender cells and/or STC receiver cells, and cultured these to the blastocyst
299 stage (Fig. 5). As expected, all chimaeric blastocysts (55/55) containing both sender and STC receiver
300 cells induced expression of mCherry, whereas no wild-type blastocysts nor blastocysts containing only
301 sender cells displayed mCherry expression (Fig. 5A,B). 12 out of 13 chimaeras containing STC receiver
302 cells alone did not express readily detectable levels of mCherry (Fig. 5B), in line with the low proportion

303 of mCherry-high cells observed *in vitro* in STC receiver cells cultured alone. All three STC clonal lines
304 reliably induced mCherry within chimaeric embryos that also contained CmGP1GH1 sender cells (Fig.
305 5B, Fig. S15). These results suggest that the SyNPL neighbour-labelling system is functional, efficient
306 and reliable *in vivo*.

307 **Spatial confinement of sender and receiver cells leads to synthetic patterning**

308 SynNotch technology has been successfully employed to generate synthetic patterns. Strategies to
309 achieve this include co-culturing cells in a low sender:receiver cell ratio in order to create 2-
310 dimensional activated receiver cell rings surrounding a clone of sender cells (Morsut et al., 2016),
311 creating self-organising cell aggregates through contact-mediated induction of adhesion molecules
312 (Toda et al., 2018), and recreating morphogen gradients through the use of anchor proteins to capture
313 diffusible receiver cell-activating signal (Toda et al., 2020).

314 We set out to test whether our clonal ESC lines could be used to generate a synthetic pattern: a stripe
315 of transgene expression at the region of contact between sender and receiver cells. To this end, we
316 plated CmGP1 sender and STC receiver cells in separate chambers of a removable multi-chamber cell
317 culture insert and allowed them to reach confluence. We then removed the insert, allowing cells to
318 grow in the space between chambers, make contact and induce transgene expression in receiver cells
319 (Fig. 6A). We assessed expression of mCherry 24 hours after initial sender:receiver contact, and
320 observed a distinct stripe of mCherry expression at the sender:receiver border (Fig. 6B). This result
321 suggest that SynNotch technology can be successfully employed in mouse ESCs to generate synthetic
322 patterns of gene expression.

323 **Harnessing modularity of SyNPL SynNotch ESCs to synthetically alter cell fate**

324 One advantage of introducing modularity to our SyNPL SynNotch system design is that we can
325 generate clonal receiver cell lines with inducible expression of any gene of interest. Having
326 characterised the system in mCherry-inducible STC receiver cells, we wished to test whether we could
327 alter receiver cell fate following interaction with sender cells by generating Neurog1-inducible receiver
328 cells.

329 The transcription factor Neurog1 (Neurogenin 1) is necessary for neural development in mice, where
330 it drives neuronal differentiation of progenitor cells (Cau et al., 2002; Ma et al., 1998; Yuan and Hassan,
331 2014). Ectopic expression of Neurog1 has been shown to lead to neuronal differentiation both in
332 ectoderm and, surprisingly, in mesoderm (Cai et al., 2000; Ma et al., 1996; Perez et al., 1999). This
333 ability of Neurog1 to induce differentiation in non-permissive conditions was exploited to drive
334 neuronal differentiation of mouse ESCs in pluripotent culture conditions (Velkey and O'Shea, 2013).
335 We therefore set out to ask whether contact-mediated induction of a *Neurog1* transgene could induce
336 neuronal differentiation specifically in receiver cells that come into contact with eGFP-expressing
337 sender cells.

338 Firstly, we generated STN (SynNotch TRE-Neurog1) receiver cells by performing RMCE at the *Rosa26*
339 landing pad in PSNB cell lines to replace the *mKate2-3xNLS* transgene with a *TRE-3xFlag-Neurog1*
340 cassette (Figs. 6C, S16A). We then tested whether we could drive contact-mediated induction of the
341 *Neurog1* transgene by co-culturing STN receiver cells with CmGP1 sender cells for 48 hours, the
342 timepoint at which we observed maximum mCherry induction in STC receiver cells (Figs. 4C,D, S13A,B).
343 We confirmed this resulted in robust induction of 3xFlag-Neurog1 in STN receiver cells compared to
344 STN receiver cells cultured alone (Fig. S16B), which suggests that PSNB landing pad cell lines can be
345 used to generate receiver cells harbouring inducible transgenes other than mCherry.

346 We then set out to test whether we could induce contact-mediated neuronal differentiation of
347 receiver cells in pluripotent culture conditions, and whether we could engineer differentiation to occur
348 in a synthetic pattern. To this end, we repeated the synthetic stripe patterning experiment described
349 above (Fig. 6A,B), using STN receiver cells in place of STC receiver cells. We assessed the expression of
350 the neuronal marker Tubb3 96 hours after initial sender:receiver contact, and observed evident
351 induction of Tubb3 and acquisition of neuronal morphology by STN receiver cells at the
352 sender:receiver border (Fig. 6D).

353 We conclude that the interaction between eGFP-expressing sender cells and STN receiver cells can
354 lead to contact-mediated *Neurog1* induction and neuronal differentiation of receiver cells in non-
355 permissive culture conditions. This demonstrates that the SyNPL system can be readily used to
356 generate clonal ESC lines for contact-mediated induction of transgenes of interest, and that these cell
357 lines can in turn be used to manipulate cell-cell interactions in order to program synthetic cell fate
358 decisions in response to contact with a particular cell population at desired locations in space.

359

360 **DISCUSSION**

361 Engineering SynNotch machinery (Morsut et al., 2016) into pluripotent cells opens up many
362 opportunities for understanding how direct cell-cell interactions between neighbouring cells can
363 control differentiation decisions, mediate cell competition (Sancho et al., 2013) and orchestrate
364 morphogenesis (Gorfinkiel and Martinez Arias, 2021) as cells differentiate in 2D or 3D culture. Mouse
365 ES cells have the unique ability to contribute to chimaeric embryos, meaning that appropriately
366 engineered cell lines can also be used to understand and control cell-cell interactions during early
367 embryonic development. There are however particular challenges associated with engineering
368 existing SynNotch technologies into pluripotent cells. Here we describe how we overcame these
369 challenges to generate the SyNPL system: a set of clonal SynNotch "sender" and "receiver" mouse ES
370 cells engineered with optimised and modular SynNotch technology. We demonstrate the utility of the
371 SyNPL system for monitoring cell-cell interactions both in culture and in early mouse embryos, and
372 show that we can use this system to engineer contact-dependent cell fate decisions at the boundary
373 between two populations of pluripotent cells.

374 **Properties of sender cells**

375 We generated sender cell lines expressing high and uniform levels of extracellular membrane-tethered
376 eGFP. This transgenic construct was previously used for SynNotch sender cells (Morsut et al., 2016;
377 Sgodda et al., 2020), and comprises eGFP fused to an N-terminal mouse IgGK signal sequence and a C-
378 terminal human PDGFRB transmembrane domain. The addition of HA and Myc tags at the N- and C-
379 termini of eGFP did not affect the ability of sender cells to induce mCherry expression in STC receiver
380 cells (Fig. S12), suggesting that the antigenic region of eGFP recognised by the LaG17 anti-GFP
381 nanobody component of the SynNotch receptor is not masked by the HA and Myc protein tags.
382 Furthermore, the LaG17 anti-GFP nanobody can also bind to *Aequorea victoria* YFP, CFP and BFP, and
383 *Aequorea macrodactyla* CFP (Fridy et al., 2014), raising the interesting possibility that transgene
384 induction in our receiver cells could be induced by sender cells expressing different membrane-
385 tethered fluorophores.

386 Mouse ESCs and mouse lines labelled with lipid anchor-tethered GFP constructs have previously been
387 described (Kondoh et al., 1999; Nowotschin et al., 2009; Rhee et al., 2006; Shioi et al., 2011). It would
388 be interesting to test if these lines could function as SynNotch sender cells; this would require
389 extracellular GFP localisation and generation of sufficient tensile force upon receptor interaction

390 (Morsut et al., 2016). GPI anchors GFP to the outer leaflet of the plasma membrane (Rhee et al., 2006;
391 Sevcsik et al., 2015); GFP-GPI-labelled cells should therefore be capable of acting as sender cells. This
392 does indeed appear to be the case in *Drosophila* (He et al., 2017).

393 **"All-in-one" locus receiver cells display suboptimal functionality**

394 Our initial attempts at generating "all-in-one" *Rosa26*-targeted receiver cells (termed SNCB+ and
395 SNCB- cells) were unsuccessful. The large variation in tagBFP expression and low proportion of
396 mCherry-inducible ESCs we saw within all of our purportedly genetically identical clonal lines suggests
397 that either widespread transgene silencing or loss of DNA occurred at the *Rosa26* safe harbour locus
398 in pluripotent cells. Furthermore, the observation that rederivation of clonal lines following
399 fluorescence-activated cell sorting of single SNCB+ and SNCB- cells led to re-establishment of the initial
400 heterogeneous distributions of fluorophore expression (Figs. S7, S8) suggests that the all-in-one design
401 is not optimal for use in pluripotent cells. We were able to overcome these problems by switching to
402 a random-integration strategy, but it is possible that inclusion of IRES-antibiotic resistance cassettes
403 and/or insulator sequences may provide an alternative route towards generating a reliable system
404 without sacrificing the all-in-one-locus approach.

405 **Landing pad ESCs provide system modularity**

406 Targeting of a landing pad to the *Rosa26* safe harbour locus has been previously characterised as an
407 efficient strategy for the rapid generation of multiple cell lines through RMCE (Seibler et al., 2005;
408 Tchorz et al., 2012; Tosti et al., 2018). We found this to be true for our cell lines harbouring a *Rosa26-*
409 *attP50-Neo-mKate2-attP50* landing pad, which we used to generate several different cell lines with
410 ease. The advantage of such a system is the ability to target different transgenes to the same genomic
411 locus in the same parental cell line. Our parental PSNB lines harbouring the *Rosa26* landing pad
412 allowed us to initially test the functionality of SynNotch in ESCs with an inducible *mCherry* transgene
413 in STC receiver cells, prior to generating genetically equivalent STN receiver cells with a *Neurog1*
414 transgene in place of *mCherry*. This modular design therefore makes it possible to readily switch
415 between using SyNPL for monitoring and profiling the consequences of defined cell-cell interactions
416 (based on contact-dependent mCherry expression) and using SyNPL for engineering contact-
417 dependent cell behaviours (based on contact-dependent expression of any cell behaviour-
418 determinant).

419 **Describing the properties of the SyNPL system**

420 We characterised various aspects of the SyNPL system that will help inform the experimental design
421 for users of these cells.

422 Previous studies have co-cultured senders and receiver cells at different ratios (ranging from 1:50 to
423 5:1), and for varying times (ranging from 10 minutes to several days) (Cho et al., 2018; Choe et al.,
424 2021; He et al., 2017; Huang et al., 2020; Luo et al., 2019; Matsunaga et al., 2020; Morsut et al., 2016;
425 Roybal et al., 2016; Sgodda et al., 2020; Srivastava et al., 2019; Toda et al., 2018; Toda et al., 2020;
426 Wang et al., 2021; Yang et al., 2020). We analysed transgene induction in STC receiver cells at 11
427 different sender:receiver cell ratios (ranging from 1:19 to 9:1), and observed that higher proportions
428 of sender cells in culture result in a higher proportion of receiver cells inducing mCherry. This is in line
429 with the results obtained by (Sgodda et al., 2020) when comparing three different sender:receiver cell
430 ratios, and with the observations of (Morsut et al., 2016), who exposed receiver cells to varying
431 concentrations of sender ligand. By finely varying the concentrations of sender ligand, Lim and
432 colleagues described the transgene induction response as sigmoidal (Morsut et al., 2016), which was

433 not evident in our data. It is however possible that by testing lower sender:receiver cell ratios this
434 might hold true in our SynNotch system too.

435 When analysing transgene expression within single samples, we found that mCherry distribution
436 follows a bimodal on/off response, indicative of the presence of receiver cells which do not interact
437 with sender cells at low sender:receiver cell ratios. This bimodal pattern of transgene induction is also
438 evident in data from Cantz and colleagues (Sgodda et al., 2020). The ability of individual sender cells
439 to induce mCherry induction in STC receiver cells (as seen in Movies 1 and 2) implies that this system
440 can be effectively employed to study the effect of interactions between receiver cells and individual
441 and/or rare sender cells in relevant model systems.

442 We performed a high-resolution study of the kinetics of mCherry induction and downregulation in STC
443 receiver cells. We observed low levels of mCherry induction in STC receiver cells following 2 hours of
444 co-culture with sender cells, provided we allowed time for subsequent protein maturation, and
445 observed maximum mCherry induction following 48 hours of co-culture. Previous studies making use
446 of lentiviral-delivered transgenes suggest that 10 minutes may be sufficient for transgene activation
447 in HEK293 receiver cells, and that 1 hour may be sufficient for transgene induction in L929 receiver
448 cells, as long as protein maturation time is allowed (Morsut et al., 2016; Sgodda et al., 2020). This is
449 significantly faster than what we observed in this study, and may be ascribable to lentiviral
450 transduction leading to higher levels of SynNotch receptor and/or integration of multiple transgene
451 copies compared to our clonal mouse ESC lines.

452 In our system, mCherry downregulation did not commence for at least 8 hours following simulated
453 loss of sender:receiver cell contact, with full loss of signal occurring after more than 40 hours. This is
454 in line with previous observations in L929 receiver cells, where inducible GFP transgene expression
455 was lost between 24 and 50 hours after sender cells were removed from culture (Morsut et al., 2016).
456 The kinetics of mCherry induction and downregulation suggest that this SynNotch system is suited for
457 the study of cell-cell interactions with a temporal range of hours rather than minutes, and that
458 "memory" of such interactions will persist for a few days. Should this persistence of mCherry signal
459 prove inconvenient for the study of particular processes, the PSNB landing pad parental cell lines can
460 be used to readily generate cell interaction reporter receiver cells harbouring destabilised inducible
461 transgenes with short half-lives.

462 **Exploring the roles of cell-cell interactions *in vivo* and *in vitro***

463 We demonstrated that our clonal mouse ESC lines can be used *in vivo* in chimaeric embryos. The ability
464 to conveniently switch between *in vitro* and *in vivo* experimentation was a key reason for us to
465 establish SynNotch technology in mouse ESCs. Both the receiver lines we generated and the parental
466 PSNB landing pad cell lines offer the power and flexibility to address questions we have so far been
467 unable to answer in *in vitro* and *in vivo* settings. For example, the system could be employed in cell
468 competition studies: STC receiver cells could be used to identify and isolate the direct neighbours of
469 eGFP-tagged "loser" cells, and profiled to study what changes are induced upon interaction with loser
470 cells in order to bring about their elimination. Receiver cells could also be engineered to express
471 candidate fitness-altering transgenes in response to interaction with eGFP-tagged wild-type sender
472 cells, as successfully demonstrated in *Drosophila* by (He et al., 2017).

473 The establishment of this system in mouse ESCs also allows to monitor and manipulate the effects of
474 cell-cell interactions in specific cell types obtained through directed differentiation. We also
475 demonstrated that our cell lines can be used to generate synthetic patterns of gene expression,
476 resulting in spatially-defined programming of cell fate. The combination of directed differentiation of

477 ESCs, spatial confinement of sender and receiver cells, and contact-mediated cell fate engineering
478 provides many possibilities for the study of cell-cell interactions in any developmental process of
479 interest.

480 **Concluding remarks**

481 Cell-cell interactions are a shared feature of the development of all multicellular organisms. Whilst the
482 particulars of these interactions vary greatly amongst eukaryotic supergroups, it is clear that they play
483 an essential role in development (Armingol et al., 2021). The Synthetic Biology field has recently
484 developed several applications to monitor cell communication, such as SynNotch (Morsut et al., 2016)
485 and derivative systems (Zhu et al., 2021), direct transfer of fluorophores to neighbouring cells
486 (Ombrato et al., 2019; Tang et al., 2020), reconstitution of a fluorophore following interaction
487 between different cell types carrying non-fluorescent fluorophore fragments (Kinoshita et al., 2020).
488 We have here demonstrated how SynNotch technology can be used to monitor and manipulate cell-
489 cell interactions in mouse ESCs and in mouse embryos. We hope that the SyNPL system will prove a
490 useful and adaptable tool for the mouse Stem Cell and Developmental Biology community.

491

492 **MATERIALS AND METHODS**

493 **Reagents**

REAGENT	SOURCE	IDENTIFIER	CONCENTRATION
Antibodies and nuclear counterstain			
Mouse monoclonal anti-Flag	Sigma-Aldrich	Cat# F3165; RRID: AB_259529	1:1000
Chicken polyclonal anti-GFP	Abcam	Cat# ab13970; RRID: AB_300798	1:1000
Goat polyclonal anti-Myc	Abcam	Cat# ab9132; RRID: AB_307033	1:1000
Mouse monoclonal anti-Myc AlexaFluor 488 conjugate	Santa Cruz	Cat# sc-40 AF488; RRID: AB_2892598	1:200
Rat monoclonal anti-mCherry	Invitrogen	Cat# M11217; RRID: AB_2536611	1:1000
Mouse monoclonal anti-Nup107 (NPC)	Abcam	Cat# ab24609; RRID: AB_448181	1:1000
Rabbit polyclonal anti-tRFP (tagBFP)	Evrogen	Cat# AB233; RRID: AB_2571743	1:1000
Mouse monoclonal anti-Tubb3	Biolegend	Cat# 801201; RRID: AB_2313773	1:1000
DRAQ7	Abcam	Cat# ab109202	1µM (IF); 300nM (flow cytometry)
Chemicals and solutions			

2-Mercaptoethanol	Gibco	Cat# 31350010	100nM
Accutase	Sigma-Aldrich	A6964	
Chorulon (hCG)	Intervet	Cat# CH-475-1	100 IU/ml
DMEM, high glucose, no glutamine, no phenol red	Gibco	Cat# 31053028	
Donkey serum	Sigma-Aldrich	Cat# D9663	3% v/v
Doxycycline hyclate	Sigma-Aldrich	Cat# D9891	1µg/ml
Dulbecco's phosphate buffered saline (PBS)	Sigma-Aldrich	Cat# D8537	
Fibronectin from bovine plasma solution	Sigma-Aldrich	Cat# F1141	
Foetal calf serum	Life Technologies	Cat# 10270106	10% v/v
Formaldehyde 37-41%	Fisher Scientific	Cat# F/1501/PB08	4% w/v
Gelatin	Sigma-Aldrich	Cat# G1890	0.1% w/v
Geneticin (G418)	Gibco	Cat# 11811031	200µg/ml
Glasgow Minimum Essential Medium	Sigma-Aldrich	Cat# G5154	
Hygromycin B	Gibco	Cat# 10687010	200µg/ml
L-Glutamine	Thermo Scientific	Cat# 25030024	2mM
Lipofectamine 3000 transfection reagent	Life Technologies	Cat# L3000008	
M2 medium	Sigma-Aldrich	Cat# M7167	
MEM Non-essential amino acids solution (100X)	Gibco	Cat# 11140050	1X
Penicillin/streptomycin	Gibco	Cat# 15140122	100 U/ml
PMSG	ProSpec	Cat# HOR-272	100 IU/ml
Prolong Gold Antifade Mountant	Thermo Fisher	Cat# P36930	
Puromycin dihydrochloride	Sigma-Aldrich	Cat# P8833	2µg/ml
Sodium pyruvate	Gibco	Cat# 11360039	1 mM
Triton X-100	Sigma-Aldrich	Cat# X100	0.1% v/v
Trypsin EDTA 0.25%	Gibco	Cat# 25200072	0.05% w/v
Tyrode's solution, acidic	Sigma-Aldrich	Cat# T1788	
Zeocin	Gibco	Cat# R25001	100µg/ml
Cell culture substrates and inserts			
3 well silicone culture insert	Ibidi	Cat# 80369	
µ-Slide 8 Well	Ibidi	Cat# 80826	
Glass coverslip, 24mm diameter	VWR	Cat# 631-1583	
Plastic flasks and plates for routine cell culture	Corning	Various	
DNA constructs			
pHR_EGFPligand	(Morsut et al., 2016)	Addgene 79129	
pHR_SFFV_LaG17_synNotch_TetRVP64	(Morsut et al., 2016)	Addgene 79128	
pDisplay-eGFP-TM	(Han et al., 2004)		

pHR_TRE-mCherry-PGK-tagBFP-WPRE	Elise Cachat, University of Edinburgh		
pRosa26-DEST-1lox	(Tosti et al., 2018)		
CAG-ϕC31 integrase	(Tosti et al., 2018)		
pENTR-2xAttP50	(Tosti et al., 2018)		
pENTR-2xAttB53	(Tosti et al., 2018)		
pPyCAG-eGFP-TM-IRES-Pac	This study		
pPyPGK-eGFP-TM-IRES-Pac	This study		
pPyCAG-HA-eGFP-Myc-TM-IRES-Pac	This study		
pPyPGK-HA-eGFP-Myc-TM-IRES-Pac	This study		
pPyPGK-Myc-LaG17-Notch1TM-tTA-IRES-Ble	This study		
pPyCAG-tagBFP-3xNLS-IRES-Hph	This study		
pENTR-attB53-Pac-bGHpA-attB53	This study		
pENTR-attB53-Pac-bGHpA-(TRE-mCherry-SV40pA)-attB53	This study		
pENTR-attB53-Pac-bGHpA-(tetO-mCherry-rBGpA)-attB53	This study		
pENTR-attB53_SNCB+_attB53	This study		
pENTR-attB53_SNCB-_attB53	This study		
pENTR-attB53-Pac-bGHpA-(TRE-3xFlag-Neurog1-SV40pA)-attB53	This study		
Cell lines			
E14Ju09 mouse ESCs (129/Ola, male)	(Hamilton and Brickman, 2014)		
CmGP1 sender mouse ESCs (129/Ola, male)	This study		
CHmGMP19 sender mouse ESCs (129/Ola, male)	This study		
CmGP1GH1 sender mouse ESCs (129/Ola, male)	This study		
E14GIP1 mouse ESCs (129/Ola, male)	This study		
EM35 mouse ESCs (129/Ola, male)	This study		
SNCB+ receiver mouse ESCs (129/Ola, male)	This study		
SNCB- receiver mouse ESCs (129/Ola, male)	This study		
35SRZ mouse ESCs (129/Ola, male)	This study		
PSNB mouse ESCs (129/Ola, male)			
PSNB-E mouse ESCs (129/Ola, male)	This study		
PSNB-tetO receiver mouse ESCs (129/Ola, male)	This study		
STC receiver mouse ESCs (129/Ola, male)	This study		

STN receiver mouse ESCs (129/Ola, male)	This study		

494

495 **Animal care and use**

496 Animal experiments were performed under the UK Home Office project license PEEC9E359, approved
497 by the Animal Welfare and Ethical Review Panel of the University of Edinburgh and within the
498 conditions of the Animals (Scientific Procedures) Act 1986.

499 **Chimaera generation**

500 C57BL/6 female mice (Charles River) were superovulated (100 IU/ml PMSG and 100 IU/ml hCG
501 intraperitoneal injections 48 hours apart) and crossed with wild-type stud male mice. Pregnant mice
502 were culled at embryonic day 2.5 (E2.5) by cervical dislocation, ovaries with oviducts were dissected
503 and collected in pre-warmed M2 medium. Oviducts were flushed using PBS and a 20-gauge needle
504 attached to a 1ml syringe and filled with PB1 (Whittingham, 1974). E2.5 embryos were collected and
505 washed in PB1, their zona pellucida was removed using acidic Tyrode's solution, and they were
506 transferred to a plate with incisions where two clumps of approximately 8 sender and 8 receiver cells
507 were added to each embryo. Embryos were then incubated at 37°C in 5% CO_2 for 48 hours prior to
508 fixation.

509 **Mouse ESC culture**

510 Mouse embryonic stem cells were routinely maintained on gelatinised culture vessels (Corning) at
511 37°C and 5% CO_2 in Glasgow Minimum Essential Medium (GMEM) supplemented with 10% foetal calf
512 serum (FCS), 100U/ml LIF (produced in-house), 100nM 2-mercaptoethanol, 1X non-essential amino
513 acids, 2mM L-Glutamine), 1mM Sodium Pyruvate (medium referred to as "ES cell culture medium" or
514 "LIF+FCS"). The medium was supplemented with 200µg/ml G418, 2µg/ml puromycin, 200µg/ml
515 hygromycin B and/or 100µg/ml zeocin as appropriate.
516 For live imaging, GMEM was replaced with phenol red-free Dulbecco's Modified Eagle Medium
517 (DMEM), with all other components of the culture medium used at identical concentrations.

518 **DNA constructs**

519 pHR_SFFV_LaG17_synNotch_TetRVP64 (Addgene plasmid #79128) (Morsut et al., 2016) and
520 pHR_EGFPligand (Addgene plasmid #79129) (Morsut et al., 2016) were kind gifts from Dr Wendell Lim
521 and Dr Leonardo Morsut. pDisplay-GFP-TM (Han et al., 2004) was a kind gift of Dr Luis Ángel Fernández
522 (CNB-CSIC). pHR_TRE-mCherry-PGK-tagBFP-WPRE was a kind gift of Dr Elise Cachat (The University of
523 Edinburgh). pRosa26-DEST-1lox, CAG-ϕC31 integrase, pENTR-2xAttP50 and pENTR-2xAttB53 (Tosti et
524 al., 2018) constructs were kind gifts of Dr Keisuke Kaji (The University of Edinburgh).

525 Untagged transmembrane eGFP constructs were generated by digesting pHR_EGFPligand with
526 XhoI+NotI, and ligating the *IgGK signal-eGFP-PDGFRB TMD* cassette into XhoI+NotI-digested *pPyCAG-*
527 *IRES-Pac* (Malaguti et al., 2019) or *pPyPGK-IRES-Pac* (Rao et al., 2020) vector backbones. HA- and Myc-
528 tagged eGFP constructs were generated by PCR-amplifying an *IgGK signal-HA-eGFP-Myc-PDGFRB TMD*
529 cassette flanked by PspXI and NotI sites from pDisplay-GFP-TM, digesting the amplicon with
530 PspXI+NotI, and ligating the insert into XhoI+NotI-digested *pPyCAG-IRES-Pac* or *pPyPGK-IRES-Pac*
531 vector backbones.

532 The *pPyPGK-CD8a signal-Myc-LaG17-Notch1 minimal transmembrane core-tTA-IRES-Ble* SynNotch
533 receptor construct was generated by PCR-amplifying a *CD8a signal-Myc-LaG17-Notch1 minimal*

534 *transmembrane core-tTA* cassette flanked by XhoI and Bsu36I sites from
535 pHR_SFFV_LaG17_synNotch_TetRVP64, digesting the amplicon with XhoI+Bsu36I, and ligating the
536 insert into a XhoI+Bsu36I-digested *pPyPGK-IRES-Ble* vector backbone. The mouse Notch1 minimal
537 transmembrane core consists of residues 1427-1752 (Uniprot: Q01705).

538 The *pPyCAG-tagBFP-3xNLS-IRES-Hph* construct was generated by PCR-amplifying a *tagBFP* cassette
539 flanked by XhoI and KasI sites from pHR_TRE-mCherry-PGK-tagBFP-WPRE, digesting the amplicon with
540 XhoI+KasI, and ligating the insert into a XhoI+NotI-digested *pPyCAG-IRES-Hph* backbone (Malaguti et
541 al., 2019) alongside oligonucleotides annealed to generate a *3xNLS* fragment with KasI and NotI
542 overhangs (Malaguti et al., 2013).

543 The *Rosa26* landing pad targeting vector was generated by Gateway Cloning (Invitrogen) of an *attL1-*
544 *attP50-Neo-SV40pA-(CAG-mKate2-3xNLS-bGHpA)-attP50-attL2* cassette into the pRosa26-DEST-1lox
545 targeting vector. Its final structure is as follows: *Rosa26 5'HA-splice acceptor-loxP-attP50-Neo-*
546 *SV40pA-(CAG-mKate2-3xNLS-bGHpA)-attP50-Rosa26 3'HA-PGK-DTA-bGHpA*. Sequence in brackets is
547 on -strand.

548 A *pENTR-attB53-Pac-bGHpA-attB53* "empty vector" construct for RMCE at the *Rosa26* locus was
549 generated by adding a *Pac-bGHpA* cassette followed by an EcoRV restriction site to pENTR-2xAttB53
550 by Gibson assembly.
551 The TRE-mCherry RMCE construct used to generated STC receiver cells from PSNB landing pad lines
552 was generated by PCR-amplifying a *TRE-mCherry-SV40pA* cassette flanked by EcoRV-AscI and EcoRV-
553 BamHI sites from pHR_TRE-mCherry-PGK-tagBFP-WPRE, digesting the amplicon with EcoRV, ligating
554 the insert into EcoRV-digested *pENTR-attB53-Pac-bGHpA-attB53* backbone, and screening for
555 insertion on the -strand. The tetO-mCherry RMCE construct used to generate PSNB-tetO cells from
556 PNSB landing pad lines was generated by PCR-amplifying a *tetO-mCherry-rBGpA* cassette flanked by
557 MluI and BamHI sites, digesting the amplicon with MluI+BamHI and ligating the insert into
558 AscI+BamHI-digested *pENTR-attB53-Pac-bGHpA-(TRE-mCherry-SV40pA)*.
559 The TRE-3xFlag-Neurog1 RMCE construct used to generate STN receiver cells from PSNB landing pad
560 lines was generated by PCR-amplifying a *3xFlag-Neurog1* cassette flanked by NdeI and MfeI sites from
561 wild-type mouse cDNA, digesting the amplicon with NdeI+MfeI and ligating the insert into NdeI+MfeI-
562 digested *pENTR-attB53-Pac-bGHpA-(TRE-mCherry-SV40pA)* backbone (in which *mCherry* is flanked by
563 NfeI and MfeI sites).

564 SNCB+ and SNCB- constructs were generated in two steps. First, the base *pENTR-attB53-Pac-bGHpA-*
565 *attB53* RMCE construct was linearised with EcoRV, and ligated with a HincII-*PGK-CD8a signal-Myc-*
566 *LaG17-Notch1 minimal transmembrane core-tTA*-HindIII fragment (digested from the SynNotch
567 receptor construct described above) and a HindIII-*bGHpA*-EcoRV fragment, and clones were screened
568 for insertion of the SynNotch receptor on the +strand. Next, the resulting construct was linearised
569 with EcoRV, and ligated with an EcoRV-*TRE-mCherry-SV40pA-PGK-tagBFP*-PacI fragment (digested
570 from pHR_TRE-mCherry-PGK-tagBFP-WPRE) and a PacI-*bGHpA*-EcoRV fragment. Correct assembly on
571 the + and - strands generated the SNCB+ and SNCB- constructs respectively.

572 Abbreviations: TMD: transmembrane domain; IRES: internal ribosome entry site; 5'/3' HA: 5'/3'
573 homology arm; SV40pA: SV40 polyadenylation signal sequence; bGHpA: bovine growth hormone
574 polyadenylation signal sequence; rBGpA: rabbit beta-globin polyadenylation signal sequence; NLS:
575 nuclear localisation signal; PGK: mouse *Pgk1* promoter; Pac: puromycin N-acetyltransferase; Hph:
576 hygromycin B phosphotransferase; Ble: bleomycin resistance gene (confers zeocin resistance); tTA:
577 tetracycline transactivator.

578 **Transfections**

579 For electroporations, 10^7 ESCs were electroporated with 100µg DNA using a BioRad GenePulser set to
580 800V/3µF. For nucleofections, $5x10^5$ ESCs were nucleofected with 5µg DNA with the Lonza P3 Primary
581 Cell Nucleofector Unit and kit, using program CG-104, and following manufacturer instructions. For
582 lipofections, 10^5 ESCs were lipofected with 3µg DNA mixed with 3µl Lipofectamine 3000 and 6µl P3000
583 solution, following manufacturer instructions. For ϕC31-mediated RMCE, equal masses of RMCE
584 constructs and CAG-ϕC31 vector were transfected.
585 Clonal ESC lines were generated by transfecting constructs of interest into ESCs, then plating cells at
586 low density onto gelatinised 9cm dishes in the absence of selection. Selective medium was added 48
587 hours post-transfection and replaced every other day. After 7-10 days, clones were manually picked,
588 dissociated, and replated into gelatinised 96-well culture plates. Clones were transferred to
589 gelatinised vessels with larger culture areas when confluent, screened as appropriate, expanded and
590 cryopreserved.

591 **Cell lines**

592 E14Ju09 ESCs are a 129/Ola male wild-type clonal line derived from E14tg2a (Hamilton and Brickman,
593 2014; Hooper et al., 1987).
594 Sender cells were generated by electroporating E14Ju09 ESCs with one of four constructs: *pPyCAG-*
595 *IgGK signal-eGFP-PDGFRB TMD-IRES-Pac* (CmGP cells), *pPyPGK-IgGK signal-eGFP-PDGFRB TMD-IRES-*
596 *Pac* (PmGP cells), *pPyCAG-IgGK signal-HA-eGFP-Myc-PDGFRB TMD-IRES-Pac* (CHmGMP cells),
597 *pPyPGK-IgGK signal-HA-eGFP-Myc-PDGFRB TMD-IRES-Pac* (PHmGMP cells). Simplified versions of the
598 constructs are displayed in Fig. 2. CmGP1GH1 sender cells were generated by lipofecting CmGP1
599 sender cells with a *pPyCAG-eGFP-IRES-Hph* construct. E14GIP1 "cytoplasmic sender" cells were
600 generated by lipofecting E14Ju09 ESCs with a *pPyCAG-eGFP-IRES-Pac* construct.
601 EM35 landing pad cells were generated by electroporating E14Ju09 ESCs with the *Rosa26* landing pad
602 targeting vector described above. Correct targeting was verified by genomic DNA PCR with the
603 following primers: Forward: GGCGGACTGGCGGGACTA, Reverse:
604 GGGACAGGATAAGTATGACATCATCAAGG. Primer locations and expected band sizes are displayed in
605 Fig. S3A. This PCR strategy was modified from that described by (Mort et al., 2014) to suit the different
606 sequence of our *Rosa26* targeting vector.
607 SNCB+ and SNCB- receiver cells were generated by electroporating EM35 ESCs with the constructs
608 depicted in Figs. S4A, S6A, and a *CAG-φC31 integrase* construct to mediate RMCE.
609 35SRZ landing pad cells were generated by electroporating EM35 landing pad cells with *pPyPGK-CD8a*
610 *signal-Myc-LaG17-Notch1 minimal transmembrane core-tTA-IRES-Ble*.
611 PSNB landing pad cell lines were generated by nucleofecting 35SRZ ESCs with a *pPyCAG-tagBFP-3xNLS-*
612 *IRES-Hph* construct. PSNB-A cells were derived from 35SRZ clone 9 (PSNB-A clone 10 renamed PSNB
613 clone A), PSNB-B cells were derived from 35SRZ clone 86 (PNSB-B clone 3 renamed PSNB clone B).
614 STC receiver cells were generated by nucleofecting PSNB ESCs with *CAG-φC31 integrase* and the
615 following RMCE construct: *attB53-Pac-bGHpA-(TRE-mCherry-SV40pA)-attB53*. Sequence in brackets is
616 on -strand. STC clone A1 was derived from PSNB clone A, STC clones B1 and B2 were derived from
617 PSNB clone B.
618 PSNB-tetO cells were generated by nucleofecting PSNB ESCs with *CAG-φC31 integrase* and the
619 following RMCE construct: *attB53-Pac-bGHpA-(tetO-mCherry-SV40pA)-attB53*. Sequence in brackets
620 is on -strand.
621 PNSB-E cells were generated by nucleofecting PSNB ESCs with *CAG-φC31 integrase* and the following
622 RMCE construct: *attB53-Pac-bGHpA-attB53*.

STN receiver cells were generated by nucleofecting PSNB clone A ESCs with *CAG-φC31 integrase* and the following RMCE construct: *attB53-Pac-bGHpA-(TRE-3xFlag-Neurog1-SV40pA)-attB53*. Sequence in brackets is on -strand.

Co-culture experiments

Sender and receiver cells were detached from culture vessels with accutase, quenched in ESC culture medium, pelleted by spinning at 300g for 3 minutes, resuspended in ESC culture medium supplemented with 2µg/ml puromycin and counted. Cells were plated at ratios described in figure legends, and at empirically determined optimal densities.
For flow cytometry experiments, cells were plated onto 12-well plates coated with 7.5µg/ml fibronectin, at the following densities: experiments carried out in the absence of doxycyline: 1h-8h: $4x10^5$ cells/well; 16h: $2.4x10^5$ cells/well; 24h: $1.6x10^5$ cells/well; 48h: $8x10^4$ cells/well; 72h: $4x10^4$ cells/well. mCherry induction with 16h doxycycline (Fig. 4F-H): 0-4h: $2.4x10^5$ cells/well; 5-8h: $1.6x10^5$ cells/well; 24h: $8x10^4$ cells/well. mCherry downregulation experiments (Fig. S14): 0h-8h: $1.6x10^5$ cells/well; 16h: $1.2x10^5$ cells/well; 24h: $8x10^4$ cells/well; 48h: $4x10^4$ cells/well.
For immunofluorescence experiments, cells were plated on flamed 24mm glass coverslips housed in a 6-well plate coated with 7.5µg/ml fibronectin.
For live imaging experiments, cells were plated onto an 8-well imaging slide coated with 7.5µg/ml fibronectin, at the following densities: mCherry induction experiments: $3x10^4$ cells/well; 0-mCherry downregulation experiments: 0-24h: $2x10^4$ cells/well; 24-48h: 10^4 cells/well. ESC culture medium was supplemented with 200µg/ml hygromycin B and 1X penicillin/streptomycin.
To test induction of 3xFlag-Neurog1 in STN receiver cells, CmGP1 sender cells and STN receiver cells were plated at a 9:1 ratio at a concentration of $2x10^5$ cells/well onto a 24mm flamed glass coverslip housed in a 6-well plate coated with 7.5µg/ml fibronectin, then fixed and stained after 48 hours.

Synthetic patterning experiments

A 24mm glass coverslip housed in a 6-well plate was coated with 7.5µg/ml fibronectin, then allowed to air dry. When fully dry, forceps were used to place a culture insert 3-well silicon chamber on top of the coverslip; downward force was carefully exerted to secure it in place. $4x10^4$ cells were plated overnight in 70µl culture medium in each of the three wells. Sender cells were plated in the central well, and receiver cells were plated in the outside wells. 2ml culture medium were added outside of the 3-well insert in order to prevent evaporation. The next day, the 2ml culture medium outside of the 3-well insert were aspirated, and the 70µl in each of the three wells were carefully removed in order not to dislodge the 3-well insert. Each well was quickly washed with 70µl PBS to get rid of any remaining cells in suspension. Forceps were used to detach the 3-well insert from the glass coverslip, and 2.5ml culture medium were added to the well. Culture medium was replaced daily. Growth of cells into the gaps between wells were monitored daily; following contact between sender and receiver cells, cells were kept in culture for a further 24 hours (STC receivers + CmGP1 senders) or a further 96 hours (STN receivers + CmGP1 senders) prior to fixation and immunofluorescence.

Flow cytometry

Cells were washed in PBS, then detached from culture vessels with accutase. They were resuspended in ice-cold PBS+10% FCS, pelleted by spinning at 300g for 3 minutes, resuspended in ice-cold PBS+10% FCS+300nM DRAQ7 and placed on ice before analysing on a BD LSRFortessa flow cytometer. Forward and side-scatter width and amplitude were used to identify single cells in suspension, dead cells were excluded by gating on DRAQ7-negative cells, and tagBFP, GFP and mCherry/mKate2 expression were then analysed using V 450/50-A, B 530/30-A, Y/G 610/20-A laser/filters combinations respectively.

667 **Immunofluorescence**

668 Cells were plated on flamed glass coverslips coated with 7.5µg/ml fibronectin and cultured as
669 indicated in figure legends. Cells were washed with PBS, fixed in 4% formaldehyde in PBS for 20
670 minutes at room temperature, then washed three times in PBS for a total of 15 minutes. Cells were
671 blocked overnight at 4°C in blocking solution (PBS+3% donkey serum+0.1% Triton X-100). Primary
672 antibodies diluted in blocking solution were added for 3 hours at room temperature, the coverslips
673 were washed 3 times in PBS for a total of 30 minutes, secondary antibodies diluted in blocking solution
674 were added for 1 hour at room temperature, the coverslips were washed 3 times in PBS for a total of
675 30 minutes. The coverslips were then mounted onto glass slides in Prolong Gold mounting medium.
676 For synthetic patterning experiments and blastocyst stainings, antibodies were incubated overnight
677 at 4°C or 37°C respectively to improve penetration. Blastocysts were imaged in PBS in an imaging
678 chamber, and scoring of mCherry-HI cells was performed manually using chimaeras containing both
679 sender and receiver cells as a reference. All imaging was performed on a Leica SP8 confocal
680 microscope with a 40X immersion lens unless otherwise indicated.

681 **Live imaging**

682 Cells to be imaged were allowed to adhere at room temperature for 15 minutes after plating, after
683 which they were placed in a 37°C 5% CO_2 humidified chamber and imaged with a widefield Nikon Ti-E
684 microscope, 20X lens, and Hamamatsu camera. Images were taken at 10 minute intervals for 24 hours,
685 and xy coordinates were saved. Following live imaging, cells were fixed and stained for fluorophore
686 expression, and imaged at the previously saved xy coordinates.

687

688 **ACKNOWLEDGEMENTS**

689 We thank Elise Cachat and Keisuke Kaji for advice and reagents; Luis Ángel Fernández for the pDisplay-
690 eGFP-TM plasmid; Dónal O'Carroll and Pedro Moreira for assistance with generating chimaeric mice;
691 Eve Moutaux for cloning initial versions of the RMCE constructs; Alexandre Veiga and Matthew French
692 for performing preliminary experiments with the original SynNotch constructs. We thank Matthieu
693 Vermeren for assistance with timelapse imaging, Fiona Rossi and Claire Cryer for flow cytometry
694 support, and Theresa O'Connor, Helen Henderson and Marilyn Thomson for cell culture support. We
695 are grateful to Val Wilson, Leonardo Morsut and members of the Lowell and Wilson labs for helpful
696 discussions.

697

698 **COMPETING INTERESTS**

699 The authors declare no competing interests.

700

701 **FUNDING**

702 This work was funded by a Wellcome Trust Senior Fellowship to SL (WT103789AIA) and a Wellcome
703 Trust Sir Henry Wellcome Fellowship to GB (WT100133).

704

705

706 **REFERENCES**

707 **Armingol, E., Officer, A., Harismendy, O. and Lewis, N. E.** (2021). Deciphering cell–cell interactions
708 and communication from gene expression. *Nature Reviews Genetics* **22**, 71–88.

709 **Arnold, S. J. and Robertson, E. J.** (2009). Making a commitment: cell lineage allocation and axis
710 patterning in the early mouse embryo. *Nature Reviews Molecular Cell Biology* **10**, 91–103.

711 **Blin, G., Wisniewski, D., Picart, C., Thery, M., Puceat, M. and Lowell, S.** (2018). Geometrical
712 confinement controls the asymmetric patterning of Brachyury in cultures of pluripotent
713 cells. *Development*.

714 **Blin, G., Sadurska, D., Migueles, R. P., Chen, N., Watson, J. A. and Lowell, S.** (2019). Nessys: A new
715 set of tools for the automated detection of nuclei within intact tissues and dense 3D
716 cultures. *PLOS Biol.* **17**, e3000388.

717 **Boggs, S. S., Gregg, R. G., Borenstein, N. and Smithies, O.** (1986). Efficient transformation and
718 frequent single-site, single-copy insertion of DNA can be obtained in mouse erythroleukemia
719 cells transformed by electroporation. *Experimental Hematology* **14**, 988–994.

720 **Bradley, A., Evans, M., Kaufman, M. H. and Robertson, E.** (1984). Formation of germ-line chimaeras
721 from embryo-derived teratocarcinoma cell lines. *Nature* **309**, 255–256.

722 **Cachat, E., Liu, W., Martin, K. C., Yuan, X., Yin, H., Hohenstein, P. and Davies, J. A.** (2016). 2- and 3-
723 dimensional synthetic large-scale de novo patterning by mammalian cells through phase
724 separation. *Sci. Rep.* **6**, 20664.

725 **Cai, L., Morrow, E. M. and Cepko, C. L.** (2000). Misexpression of basic helix-loop-helix genes in the
726 murine cerebral cortex affects cell fate choices and neuronal survival. *Development* **127**,
727 3021–3030.

728 **Cau, E., Casarosa, S. and Guillemot, F.** (2002). Mash1 and Ngn1 control distinct steps of
729 determination and differentiation in the olfactory sensory neuron lineage. *Development* **129**,
730 1871–1880.

731 **Charrier, S., Ferrand, M., Zerbato, M., Précigout, G., Viornery, A., Bucher-Laurent, S., Benkhelifa-**
732 **Ziyyat, S., Merten, O. W., Perea, J. and Galy, A.** (2011). Quantification of lentiviral vector
733 copy numbers in individual hematopoietic colony-forming cells shows vector dose-
734 dependent effects on the frequency and level of transduction. *Gene Therapy* **18**, 479–487.

735 **Chen, C., Krohn, J., Bhattacharya, S. and Davies, B.** (2011). A Comparison of Exogenous Promoter
736 Activity at the ROSA26 Locus Using a PhiC31 Integrase Mediated Cassette Exchange
737 Approach in Mouse ES Cells. *PLOS ONE* **6**, e23376.

738 **Cho, J. H., Okuma, A., Al-Rubaye, D., Intisar, E., Junghans, R. P. and Wong, W. W.** (2018).
739 Engineering Axl specific CAR and SynNotch receptor for cancer therapy. *Scientific Reports* **8**,
740 3846.

741 **Choe, J. H., Watchmaker, P. B., Simic, M. S., Gilbert, R. D., Li, A. W., Krasnow, N. A., Downey, K. M.,**
742 **Yu, W., Carrera, D. A., Celli, A., et al.** (2021). SynNotch-CAR T cells overcome challenges of
743 specificity, heterogeneity, and persistence in treating glioblastoma. *Sci Transl Med* **13**,.

744 **Davies, J.** (2017). Using synthetic biology to explore principles of development. *Development* **144**,
745 1146–1158.

746 **De Los Angeles, A., Ferrari, F., Xi, R., Fujiwara, Y., Benvenisty, N., Deng, H., Hochedlinger, K.,**
747 **Jaenisch, R., Lee, S., Leitch, H. G., et al.** (2015). Hallmarks of pluripotency. *Nature* **525**, 469–
748 478.

749 **Dias, A. S., Almeida, I. de, Belmonte, J. M., Glazier, J. A. and Stern, C. D.** (2014). Somites Without a
750 Clock. *Science* **343**, 791–795.

751 **Ebrahimkhani, M. R. and Ebisuya, M.** (2019). Synthetic developmental biology: build and control
752 multicellular systems. *Curr. Opin. Chem. Biol.* **52**, 9–15.

753 **Evans, M. J. and Kaufman, M. H.** (1981). Establishment in culture of pluripotential cells from mouse
754 embryos. *Nature* **292**, 154–156.

755 **Fischer, S. C., Corujo-Simon, E., Lilao-Garzon, J., Stelzer, E. H. K. and Muñoz-Descalzo, S.** (2020). The
756 transition from local to global patterns governs the differentiation of mouse blastocysts.
757 *PLOS ONE* **15**, e0233030.

758 **Forsyth, J. E., Al-Anbaki, A. H., Fuente, R. de la, Modare, N., Perez-Cortes, D., Rivera, I., Kelly, R. S.,**
759 **Cotter, S. and Plusa, B.** (2021). IVEN: A quantitative tool to describe 3D cell position and
760 neighbourhood reveals architectural changes in FGF4-treated preimplantation embryos.
761 *PLOS Biology* **19**, e3001345.

762 **Fridy, P. C., Li, Y., Keegan, S., Thompson, M. K., Nudelman, I., Scheid, J. F., Oeffinger, M.,**
763 **Nussenzweig, M. C., Fenyö, D., Chait, B. T., et al.** (2014). A robust pipeline for rapid
764 production of versatile nanobody repertoires. *Nature Methods* **11**, 1253–1260.

765 **Friedrich, G. and Soriano, P.** (1991). Promoter traps in embryonic stem cells: a genetic screen to
766 identify and mutate developmental genes in mice. *Gene Dev* **5**, 1513–1523.

767 **Gorfinkiel, N. and Martinez Arias, A.** (2021). The cell in the age of the genomic revolution: Cell
768 Regulatory Networks. *Cells & Development* 203720.

769 **Gossen, M. and Bujard, H.** (1992). Tight control of gene expression in mammalian cells by
770 tetracycline-responsive promoters. *Proceedings of the National Academy of Sciences* **89**,
771 5547–5551.

772 **Gurdon, J. B.** (1987). Embryonic induction — molecular prospects. *Development* **99**, 285–306.

773 **Hamilton, W. B. and Brickman, J. M.** (2014). Erk signaling suppresses embryonic stem cell self-
774 renewal to specify endoderm. *Cell Reports* **9**, 2056–2070.

775 **Han, H.-J., Park, S.-G., Kim, S.-H., Hwang, S.-Y., Han, J., Traicoff, J., Kho, W.-G. and Chung, J.-Y.**
776 (2004). Epidermal growth factor-like motifs 1 and 2 of Plasmodium vivax merozoite surface
777 protein 1 are critical domains in erythrocyte invasion. *Biochemical and Biophysical Research*
778 *Communications* **320**, 563–570.

779 **He, L., Huang, J. and Perrimon, N.** (2017). Development of an optimized synthetic Notch receptor as
780 an in vivo cell–cell contact sensor. *Proc. Natl. Acad. Sci.* **114**, 5467–5472.

781 **Herbst, F., Ball, C. R., Tuorto, F., Nowrouzi, A., Wang, W., Zavidij, O., Dieter, S. M., Fessler, S.,**
782 **Hoeven, F. van der, Kloz, U., et al.** (2012). Extensive Methylation of Promoter Sequences
783 Silences Lentiviral Transgene Expression During Stem Cell Differentiation In Vivo. *Molecular*
784 *Therapy* **20**, 1014–1021.

785 **Ho, C. and Morsut, L.** (2021). Novel synthetic biology approaches for developmental systems. *Stem*
786 *Cell Reports* **16**, 1051–1064.

787 **Hong, S., Hwang, D.-Y., Yoon, S., Isacson, O., Ramezani, A., Hawley, R. G. and Kim, K.-S.** (2007).
788 Functional Analysis of Various Promoters in Lentiviral Vectors at Different Stages of In Vitro
789 Differentiation of Mouse Embryonic Stem Cells. *Molecular Therapy* **15**, 1630–1639.

790 **Hooper, M., Hardy, K., Handyside, A., Hunter, S. and Monk, M.** (1987). HPRT-deficient (Lesch–
791 Nyhan) mouse embryos derived from germline colonization by cultured cells. *Nature* **326**,
792 292–295.

793 **Huang, J., Zhou, W., Dong, W., Watson, A. M. and Hong, Y.** (2009). Directed, efficient, and versatile
794 modifications of the Drosophila genome by genomic engineering. *Proceedings of the*
795 *National Academy of Sciences* **106**, 8284–8289.

796 **Huang, H., Zhang, X., Lv, J., Yang, H., Wang, X., Ma, S., Shao, R., Peng, X., Lin, Y. and Rong, Z.**
797 (2020). Cell-cell contact-induced gene editing/activation in mammalian cells using a
798 synNotch-CRISPR/Cas9 system. *Protein & Cell* **11**, 299–303.

799 **Johnson, M. H. and Ziomek, C. A.** (1983). Cell interactions influence the fate of mouse blastomeres
800 undergoing the transition from the 16- to the 32-cell stage. *Developmental Biology* **95**, 211–
801 218.

802 **Kinoshita, M. and Smith, A.** (2018). Pluripotency Deconstructed. *Development, Growth &*
803 *Differentiation* **60**, 44–52.

804 **Kinoshita, N., Huang, A. J. Y., McHugh, T. J., Miyawaki, A. and Shimogori, T.** (2020). Diffusible
805 GRAPHIC to visualize morphology of cells after specific cell–cell contact. *Scientific Reports* **10**,
806 14437.

807 **Kondoh, G., Gao, X.-H., Nakano, Y., Koike, H., Yamada, S., Okabe, M. and Takeda, J.** (1999). Tissue-
808 inherent fate of GPI revealed by GPI-anchored GFP transgenesis. *FEBS Letters* **458**, 299–303.

809 **Luo, H., Wu, X., Sun, R., Su, J., Wang, Y., Dong, Y., Shi, B., Sun, Y., Jiang, H. and Li, Z.** (2019). Target-
810 Dependent Expression of IL12 by synNotch Receptor-Engineered NK92 Cells Increases the
811 Antitumor Activities of CAR-T Cells. *Frontiers in Oncology* **9**,.

812 **Ma, Q., Kintner, C. and Anderson, D. J.** (1996). Identification of neurogenin, a Vertebrate Neuronal
813 Determination Gene. *Cell* **87**, 43–52.

814 **Ma, Q., Chen, Z., Barrantes, I. del B., Pompa, J. L. de la and Anderson, D. J.** (1998). neurogenin1 Is
815 Essential for the Determination of Neuronal Precursors for Proximal Cranial Sensory Ganglia.
816 *Neuron* **20**, 469–482.

817 **Malaguti, M., Nistor, P. A., Blin, G., Pegg, A., Zhou, X. and Lowell, S.** (2013). Bone morphogenic
818 protein signalling suppresses differentiation of pluripotent cells by maintaining expression of
819 E-Cadherin. *eLife* **2**, e01197.

820 **Malaguti, M., Migueles, R. P., Blin, G., Lin, C.-Y. and Lowell, S.** (2019). Id1 Stabilizes Epiblast Identity
821 by Sensing Delays in Nodal Activation and Adjusting the Timing of Differentiation. *Dev. Cell*
822 **50**, 462–477.e5.

823 **Martin, G. R.** (1981). Isolation of a pluripotent cell line from early mouse embryos cultured in
824 medium conditioned by teratocarcinoma stem cells. *Proceedings of the National Academy of*
825 *Sciences* **78**, 7634–7638.

826 **Matsuda, M., Koga, M., Woltjen, K., Nishida, E. and Ebisuya, M.** (2015). Synthetic lateral inhibition
827 governs cell-type bifurcation with robust ratios. *Nat Commun* **6**, 6195.

828 **Matsunaga, S., Jeremiah, S. S., Miyakawa, K., Kurotaki, D., Shizukuishi, S., Watashi, K., Nishitsuji,**
829 **H., Kimura, H., Tamura, T., Yamamoto, N., et al.** (2020). Engineering Cellular Biosensors
830 with Customizable Antiviral Responses Targeting Hepatitis B Virus. *iScience* **23**,.

831 **McBurney, M. W., Sutherland, L. C., Adra, C. N., Leclair, B., Rudnicki, M. A. and Jardine, K.** (1991).
832 The mouse Pgk-1 gene promoter contains an upstream activator sequence. *Nucleic Acids*
833 *Research* **19**, 5755–5761.

834 **Morsut, L., Roybal, K. T., Xiong, X., Gordley, R. M., Coyle, S. M., Thomson, M. and Lim, W. A.**
835 (2016). Engineering Customized Cell Sensing and Response Behaviors Using Synthetic Notch
836 Receptors. *Cell* **164**, 780–791.

837 **Mort, R. L., Ford, M. J., Sakaue-Sawano, A., Lindstrom, N. O., Casadio, A., Douglas, A. T., Keighren,**
838 **M. A., Hohenstein, P., Miyawaki, A. and Jackson, I. J.** (2014). Fucci2a: A bicistronic cell cycle
839 reporter that allows Cre mediated tissue specific expression in mice. *Cell Cycle* **13**, 2681–
840 2696.

841 **Nishida-Aoki, N. and Gujral, T. S.** (2019). Emerging approaches to study cell-cell interactions in
842 tumor microenvironment. *Oncotarget* **10**, 785–797.

843 **Niwa, H., Yamamura, K. and Miyazaki, J.** (1991). Efficient selection for high-expression transfectants
844 with a novel eukaryotic vector. *Gene* **108**, 193–199.

845 **Nowotschin, S. and Hadjantonakis, A.-K.** (2010). Cellular dynamics in the early mouse embryo: from
846 axis formation to gastrulation. *Current Opinion in Genetics & Development* **20**, 420–427.

847 **Nowotschin, S., Eakin, G. S. and Hadjantonakis, A.-K.** (2009). Dual transgene strategy for live
848 visualization of chromatin and plasma membrane dynamics in murine embryonic stem cells
849 and embryonic tissues. *genesis* **47**, 330–336.

850 **Ombrato, L., Nolan, E., Kurelac, I., Mavousian, A., Bridgeman, V. L., Heinze, I., Chakravarty, P.,**
851 **Horswell, S., Gonzalez-Gualda, E., Matacchione, G., et al.** (2019). Metastatic-niche labelling
852 reveals parenchymal cells with stem features. *Nature* **572**, 603–608.

853 **Pera, M. F. and Tam, P. P. L.** (2010). Extrinsic regulation of pluripotent stem cells. *Nature* **465**, 713–
854 720.

855 **Perez, S. E., Rebelo, S. and Anderson, D. J.** (1999). Early specification of sensory neuron fate
856 revealed by expression and function of neurogenins in the chick embryo. *Development* **126**,
857 1715–1728.

858 **Pfaff, N., Lachmann, N., Ackermann, M., Kohlscheen, S., Brendel, C., Maetzig, T., Niemann, H.,**
859 **Antoniou, M. N., Grez, M., Schambach, A., et al.** (2013). A ubiquitous chromatin opening
860 element prevents transgene silencing in pluripotent stem cells and their differentiated
861 progeny. *STEM CELLS* **31**, 488–499.

862 **Pfeifer, A., Ikawa, M., Dayn, Y. and Verma, I. M.** (2002). Transgenesis by lentiviral vectors: lack of
863 gene silencing in mammalian embryonic stem cells and preimplantation embryos.
864 *Proceedings of the National Academy of Sciences of the United States of America* **99**, 2140–
865 2145.

866 **Posfai, E., Lanner, F., Mulas, C. and Leitch, H. G.** (2021). All models are wrong, but some are useful:
867 Establishing standards for stem cell-based embryo models. *Stem Cell Reports* **16**, 1117–1141.

868 **Rao, C., Malaguti, M., Mason, J. O. and Lowell, S.** (2020). The transcription factor E2A drives neural
869 differentiation in pluripotent cells. *Development*.

870 **Rhee, J. M., Pirity, M. K., Lackan, C. S., Long, J. Z., Kondoh, G., Takeda, J. and Hadjantonakis, A.-K.**
871 (2006). In vivo imaging and differential localization of lipid-modified GFP-variant fusions in
872 embryonic stem cells and mice. *genesis* **44**, 202–218.

873 **Rossant, J. and Tam, P. P. L.** (2009). Blastocyst lineage formation, early embryonic asymmetries and
874 axis patterning in the mouse. *Development* **136**, 701–713.

875 **Roybal, K. T., Williams, J. Z., Morsut, L., Rupp, L. J., Kolinko, I., Choe, J. H., Walker, W. J., McNally,**
876 **K. A. and Lim, W. A.** (2016). Engineering T Cells with Customized Therapeutic Response
877 Programs Using Synthetic Notch Receptors. *Cell* **167**, 419–432.e16.

878 **Sancho, M., Di-Gregorio, A., George, N., Pozzi, S., Sánchez, J. M., Pernaute, B. and Rodríguez, T. A.**
879 (2013). Competitive Interactions Eliminate Unfit Embryonic Stem Cells at the Onset of
880 Differentiation. *Developmental Cell* **26**, 19–30.

881 **Santorelli, M., Lam, C. and Morsut, L.** (2019). Synthetic development: building mammalian
882 multicellular structures with artificial genetic programs. *Curr Opin Biotechnol* **59**, 130–140.

883 **Schlissel, G. and Li, P.** (2020). Synthetic Developmental Biology: Understanding Through
884 Reconstitution. *Annu. Rev. Cell Dev. Biol.* **36**, 339–357.

885 **Schultz, R. M.** (1985). Roles of Cell-to-Cell Communication in Development. *Biology of Reproduction*
886 **32**, 27–42.

887 **Seibler, J., Küter-Luks, B., Kern, H., Streu, S., Plum, L., Mauer, J., Kühn, R., Brüning, J. C. and**
888 **Schwenk, F.** (2005). Single copy shRNA configuration for ubiquitous gene knockdown in
889 mice. *Nucleic Acids Research* **33**, e67–e67.

890 **Sekine, R., Shibata, T. and Ebisuya, M.** (2018). Synthetic mammalian pattern formation driven by
891 differential diffusivity of Nodal and Lefty. *Nat Commun* **9**, 5456.

892 **Sevcsik, E., Brameshuber, M., Fölser, M., Weghuber, J., Honigmann, A. and Schütz, G. J.** (2015).
893 GPI-anchored proteins do not reside in ordered domains in the live cell plasma membrane.
894 *Nature Communications* **6**, 6969.

895 **Sgodda, M., Alfken, S., Schambach, A., Eggenschwiler, R., Fidzinski, P., Hummel, M. and Cantz, T.**
896 (2020). Synthetic Notch-Receptor-Mediated Transmission of a Transient Signal into
897 Permanent Information via CRISPR/Cas9-Based Genome Editing. *Cells* **9**, 1929.

898 **Shcherbo, D., Murphy, C. S., Ermakova, G. V., Solovieva, E. A., Chepurnykh, T. V., Shcheglov, A. S.,**
899 **Verkhusha, V. V., Pletnev, V. Z., Hazelwood, K. L., Roche, P. M., et al.** (2009). Far-red
900 fluorescent tags for protein imaging in living tissues. *Biochemical Journal* **418**, 567–574.

901 **Shioi, G., Kiyonari, H., Abe, T., Nakao, K., Fujimori, T., Jang, C.-W., Huang, C.-C., Akiyama, H.,**
902 **Behringer, R. R. and Aizawa, S.** (2011). A mouse reporter line to conditionally mark nuclei
903 and cell membranes for in vivo live-imaging. *Genesis* **49**, 570–578.

904 **Smithies, O., Gregg, R. G., Boggs, S. S., Koralewski, M. A. and Kucherlapati, R. S.** (1985). Insertion of
905 DNA sequences into the human chromosomal ß-globin locus by homologous recombination.
906 *Nature* **317**, 230–234.

907 **Srivastava, S., Salter, A. I., Liggitt, D., Yechan-Gunja, S., Sarvothama, M., Cooper, K., Smythe, K. S.,**
908 **Dudakov, J. A., Pierce, R. H., Rader, C., et al.** (2019). Logic-Gated ROR1 Chimeric Antigen
909 Receptor Expression Rescues T Cell-Mediated Toxicity to Normal Tissues and Enables
910 Selective Tumor Targeting. *Cancer Cell* **35**, 489–503.e8.

911 **Stern, C.** (1936). Somatic Crossing Over and Segregation in Drosophila Melanogaster. *Genetics* **21**,
912 625–730.

913 **Tam, P. P. L. and Loebel, D. A. F.** (2007). Gene function in mouse embryogenesis: get set for
914 gastrulation. *Nature Reviews Genetics* **8**, 368–381.

915 **Tang, R., Murray, C. W., Linde, I. L., Kramer, N. J., Lyu, Z., Tsai, M. K., Chen, L. C., Cai, H., Gitler, A.**
916 **D., Engleman, E., et al.** (2020). A versatile system to record cell-cell interactions. *eLife* **9**,
917 e61080.

918 **Tchorz, J. S., Suply, T., Ksiazek, I., Giachino, C., Cloëtta, D., Danzer, C.-P., Doll, T., Isken, A.,**
919 **Lemaistre, M., Taylor, V., et al.** (2012). A Modified RMCE-Compatible Rosa26 Locus for the
920 Expression of Transgenes from Exogenous Promoters. *PLOS ONE* **7**, e30011.

921 **Toda, S., Blauch, L. R., Tang, S. K. Y., Morsut, L. and Lim, W. A.** (2018). Programming self-organizing
922 multicellular structures with synthetic cell-cell signaling. *Science* **361**, 156–162.

923 **Toda, S., McKeithan, W. L., Hakkinen, T. J., Lopez, P., Klein, O. D. and Lim, W. A.** (2020). Engineering
924 synthetic morphogen systems that can program multicellular patterning. *Science* **370**, 327–
925 331.

926 **Tosti, L., Ashmore, J., Tan, B. S. N., Carbone, B., Mistri, T. K., Wilson, V., Tomlinson, S. R. and Kaji,**
927 **K.** (2018). Mapping transcription factor occupancy using minimal numbers of cells in vitro
928 and in vivo. *Genome Research* **28**, 592–605.

929 **Toth, T., Balassa, T., Bara, N., Kovacs, F., Kriston, A., Molnar, C., Haracska, L., Sukosd, F. and**
930 **Horvath, P.** (2018). Environmental properties of cells improve machine learning-based
931 phenotype recognition accuracy. *Scientific Reports* **8**, 10085.

932 **Velkey, J. M. and O'Shea, K. S.** (2013). Expression of Neurogenin 1 in Mouse Embryonic Stem Cells
933 Directs the Differentiation of Neuronal Precursors and Identifies Unique Patterns of Down-
934 stream Gene Expression. *Developmental Dynamics* **242**, 230–253.

935 **Wang, L., Long, J., Chen, H., Sun, S., Lv, K., Li, Q. and Wang, X.** (2021). Manipulation of focal Wnt
936 activity via synthetic cells in a double-humanized zebrafish model of tumorigenesis.
937 *International Journal of Cancer* **148**, 2815–2824.

938 **Whittingham, D. G.** (1974). Embryo banks in the future of developmental genetics. *Genetics* **78**,
939 395–402.

940 **Wu, G., Liu, N., Rittelmeyer, I., Sharma, A. D., Sgodda, M., Zaehres, H., Bleidißel, M., Greber, B.,**
941 **Gentile, L., Han, D. W., et al.** (2011). Generation of Healthy Mice from Gene-Corrected
942 Disease-Specific Induced Pluripotent Stem Cells. *PLOS Biology* **9**, e1001099.

943 **Yang, Z., Yu, Z., Cai, Y., Du, R. and Cai, L.** (2020). Engineering of an enhanced synthetic Notch
944 receptor by reducing ligand-independent activation. *Communications Biology* **3**, 1–7.

945 **Yang, B. A., Westerhof, T. M., Sabin, K., Merajver, S. D. and Aguilar, C. A.** (2021). Engineered Tools
946 to Study Intercellular Communication. *Advanced Science* **8**, 2002825.

947 **Yuan, L. and Hassan, B. A.** (2014). Neurogenins in brain development and disease: An overview.
948 *Archives of Biochemistry and Biophysics* **558**, 10–13.

949 **Zhu, I., Liu, R., Hyrenius-Wittsten, A., Piraner, D. I., Alavi, J., Israni, D. V., Khalil, A. S. and Roybal, K.**
950 **T.** (2021). Design and modular assembly of synthetic intramembrane proteolysis receptors
951 for custom gene regulation in therapeutic cells. *bioRxiv* 2021.05.21.445218.

952

953 **FIGURE LEGENDS**

954 **Figure 1. Diagram of SynNotch cell-cell interaction reporter ES cells.**
955 (A) Sender cells express membrane-tethered extracellular eGFP from a ubiquitous promoter. (B)
956 Receiver cells contain a *TRE-mCherry* transgene, express *tagBFP-3xNLS* from a ubiquitous promoter,
957 and express a SynNotch receptor from a ubiquitous promoter. The SynNotch receptor is comprised
958 of an extracellular LaG17 anti-GFP nanobody, the core transmembrane region of Notch1 (containing
959 proteolytic cleavage sites), and an intracellular tTA. (C) Upon interaction of the eGFP on a sender cell
960 with the SynNotch receptor, the Notch1 core domain is cleaved, releasing the tTA, which can
961 translocate into the nucleus, bind the TRE element, and drive *mCherry* transcription.

962 **Figure 2. Screening of clonal sender ESC lines.**
963 (A-D) Diagram of the constructs used to generate eGFP sender cell lines. (E) Median eGFP intensity
964 and (G) percentage eGFP-positive cells in untagged eGFP sender cells. Parental wild-type cells are
965 included as a negative control. 5000 cells were analysed for each clone. (F) Median eGFP intensity
966 and (H) percentage eGFP-positive cells in HA- and Myc-tagged eGFP sender cells. Parental wild-type
967 cells are included as a negative control. 15000 cells were analysed for each clone. Analyses were
968 performed separately from those in (E), median intensities are not directly comparable. (I)
969 Comparison of eGFP distributions in parental wild-type cells, CmGP1 and CHmGMP19 sender cells.
970 85000 cells were analysed for each sample. (J-K) Immunofluorescence of (J) CmGP1 and (K)
971 CHmGMP19 sender cells. Scale bar: 30µm. NPC: nuclear pore complex. A.F.U.: arbitrary fluorescence
972 units.

973 **Figure 3. Generation of clonal cell-cell interaction reporter STC receiver cells.**
974 (A) Summary of transgenes stably integrated into the genome of STC clonal ESC lines. (B-C) Flow
975 cytometry analysis of mCherry and tagBFP-3xNLS expression in (B) wild-type and (C) control PSNBB-E
976 cells containing all SyNPL receiver constructs except for the TRE-mCherry cassette. These control cell

977 lines were used to set gates for tagBFP- and mCherry-positivity. (D) Immunofluorescence of STC
978 clones A1, B1 and B2 co-cultured with CmGP1 sender cells for 24 hours (1:3 sender:receiver cell
979 ratio). Scale bar: 30µm. (E-H) Flow cytometry analysis of mCherry and tagBFP-3xNLS expression in
980 STC receiver cells cultured alone or in the presence of indicated eGFP-expressing cell lines (9:1
981 sender:receiver cell ratio). The mCherry-HI gate displayed in figure was set based on mCherry
982 distribution in STC receiver cells cultured alone.
983 For panels (B,C,E-H) percentages of cells in each gate are indicated. 11000 cells were analysed for
984 each sample. Diagrams depicting the transgenes present in each cell type and expected mCherry and
985 tagBFP-3xNLS expression patterns are displayed next to flow cytometry plots.

986 **Figure 4. Kinetics of mCherry induction in STC receiver cells.**
987 (A) Stills from Movie 1 displaying mCherry and eGFP expression in STC clone A1 receiver cells co-
988 cultured with CmGP1GH1 sender cells (1:1 sender:receiver cell ratio). Immuofluorescence of cells
989 after 24 hours of filming is displayed as a 24 hour timepoint, and includes tagBFP-3xNLS signal in
990 place of a brightfield image. Scale bar: 30µm. Yellow arrowheads: initial STC receiver cell contact
991 with sender cells, onset of mCherry expression, cell descendants at 24 hours. Magenta arrowheads:
992 STC receiver cell not making contact with sender cells, cell descendants at 24 hours. Cyan
993 arrowhead: initial STC receiver cell contact with sender cell, cell descendant at 24 hours.
994 (B) Experimental setup to analyse kinetics of mCherry upregulation in STC receiver cells by flow
995 cytometry.
996 (C) Percentage of mCherry-HI STC receiver cells following co-culture with CmGP1 sender cells for the
997 indicated amount of time (9:1 sender:receiver cell ratio). Data presented as mean ± standard
998 deviation of three independent experiments. A minimum of 8000 cells were analysed for each
999 sample. The mCherry-HI gate was set based on mCherry distribution in STC receiver cells cultured
1000 alone.
1001 (D) Distribution of mCherry fluorescence in STC clone A1 receiver cells following co-culture with
1002 CmGP1 sender cells for the indicated amount of time (9:1 sender:receiver cell ratio). Data from a
1003 single experiment, representative of three biological replicates. STC clone A1 cells cultured alone
1004 ("0h") are displayed as a shaded black histogram in all panels. 10000 cells were analysed for each
1005 sample.
1006 (E) Stills from Movie 2 displaying mCherry and eGFP expression in STC clone A1 receiver cells co-
1007 cultured with CmGP1GH1 sender cells (1:1 sender:receiver cell ratio). Immuofluorescence of cells
1008 after 24 hours of filming is displayed as a 24 hour timepoint, and includes tagBFP-3xNLS signal in
1009 place of a brightfield image. Scale bar: 30µm. White arrowheads label an STC receiver cell in contact
1010 with sender cells for 7 hours, which then loses contact with sender cells between the 8 and 20 hour
1011 timepoints whilst its levels of mCherry keep increasing.(F) Experimental setup to analyse kinetics of
1012 mCherry upregulation in STC receiver cells by flow cytometry, allowing time for protein maturation.
1013 Following sender:receiver cell co-culture for 0-24 hours, 1µg/ml doxycycline (dox) was added to the
1014 culture medium for a further 16 hours in order to inhibit tTA-mediated *mCherry* transcription, and
1015 allow translation and folding of previously transcribed *mCherry*.
1016 (G) Percentage of mCherry-HI STC receiver cells after co-culture with CmGP1 sender cells for the
1017 indicated amount of time and following a further 16 hours of doxycycline treatment (9:1
1018 sender:receiver cell ratio). Data presented as mean ± standard deviation of three independent
1019 experiments. A minimum of 8000 cells were analysed for each sample. The mCherry-HI gate was set
1020 based on mCherry distribution in STC receiver cells cultured alone in doxycycline for 16 hours.
1021 (H) Distribution of mCherry fluorescence in STC clone A1 receiver cells following co-culture with
1022 CmGP1 sender cells for the indicated amount of time and 16 hours doxycycline treatment (9:1
1023 sender:receiver cell ratio). Data from a single experiment, representative of three biological
1024 replicates. STC clone A1 cells plated with CmGP1 sender cells in doxycycline-containing medium for
1025 16 hours ("0h") are displayed as a shaded black histogram in all panels. 10000 cells were analysed
1026 for each sample.
1027

1028 **Figure 5. Contact-mediated induction of mCherry in chimaeric blastocysts.**
1029 (A) Chimaeric blastocysts containing STC clone B2 receiver cells and/or CmGP1GH1 sender cells. The
1030 images of the three embryos were taken from the same z-plane of a confocal stack and come from a
1031 single field of view. Nuclei were counterstained with DRAQ7. Scale bars: 30µm. (B) Quantification of
1032 embryos containing cells expressing readily detectable levels of mCherry ("mCherry-HI") across all
1033 experiments. Embryos containing both sender and receiver cells were used as a reference for scoring
1034 sender-only chimaeras, receiver-only chimaeras, and wild-type embryos.

1035 **Figure 6. Contact-mediated synthetic patterning of gene expression and fate programming.**
1036 (A) Diagram illustrating synthetic patterning strategy: sender and receiver cells are grown to
1037 confluence in separate chambers of a multi-chamber culture insert. The insert is removed and cells
1038 are allowed to proliferate until they come into contact, which induces transgene expression in
1039 receiver cells in a stripe pattern. (B) Synthetic striped pattern of mCherry induction in STC clone B1
1040 receiver ESCs in contact with CmGP1 sender ESCs. eGFP, tagBFP, mCherry immunofluorescence. (C)
1041 Summary of transgenes stably integrated into the genome of *Neurog1*-inducible STN clonal ESC lines.
1042 (D) Synthetic striped pattern of neuronal differentiation of STN receiver ES cells in contact with
1043 CmGP1 sender ESCs. eGFP, tagBFP, Tubb3 immunofluorescence. Scale bars: 30µm.

FIGURE 1

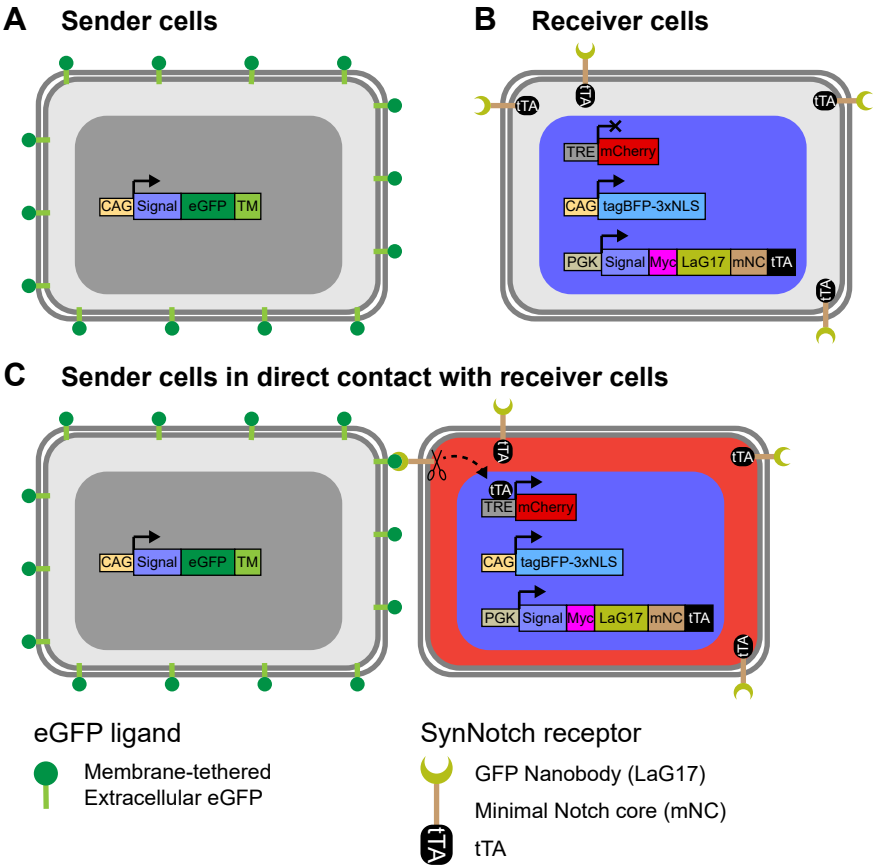
A
Sender cells
CAG
Signal
eGFP
TM
B
Receiver cells
tTA
TRE
mCherry
CAG
tagBFP-3xNLS
PGK
Signal
Myc
LaG17
mNC
tTA
C
Sender cells in direct contact with receiver cells
eGFP ligand
Membrane-tethered
Extracellular eGFP
SynNotch receptor
GFP Nanobody (LaG17)
Minimal Notch core (mNC)
tTA

FIGURE 2

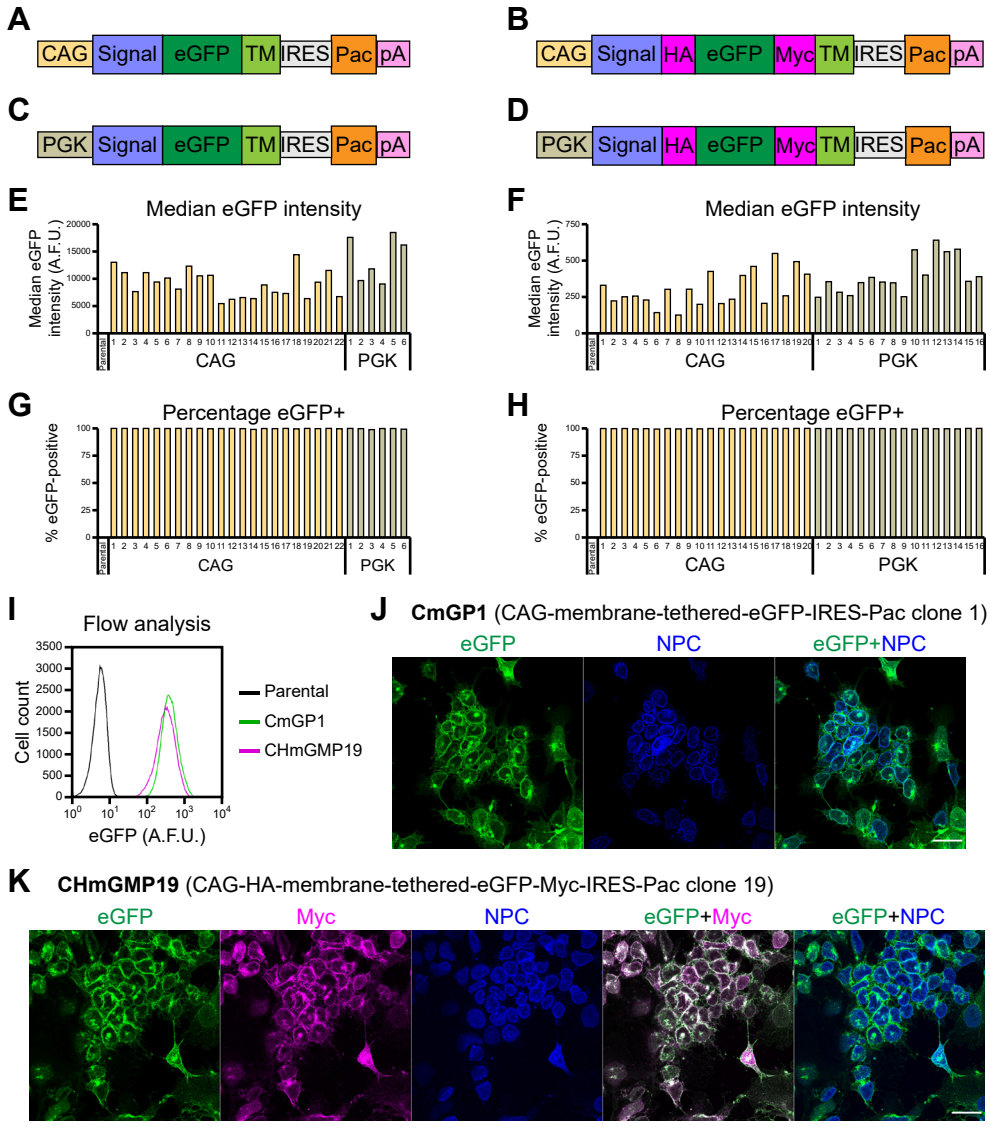

K **CHmGMP19** (CAG-HA-membrane-tethered-eGFP-Myc-IRES-Pac clone 19)

FIGURE 3

A

STC receiver cells (SynNotch-TRE-mCherry)

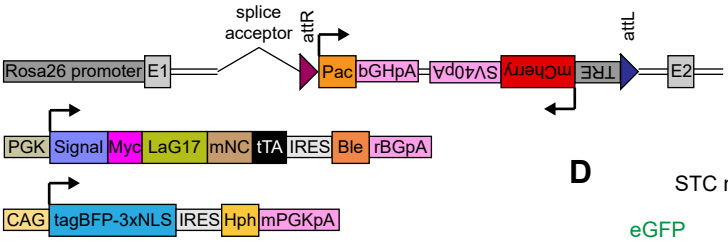

B

Wild-type

C

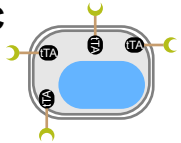

EV control "receivers"

Flow analysis of GFP- cells

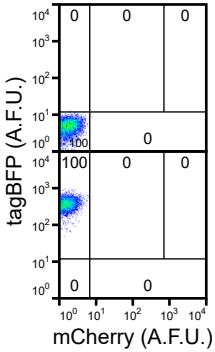

D

STC receivers + CmGP1 senders

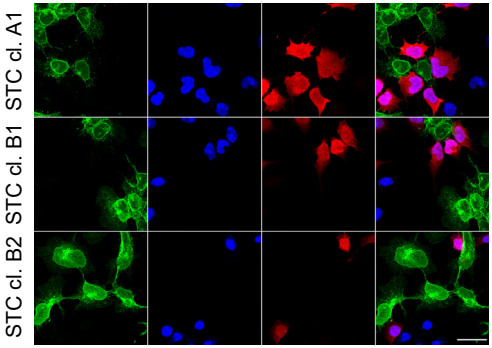

E

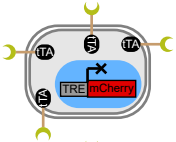

STC receivers

F

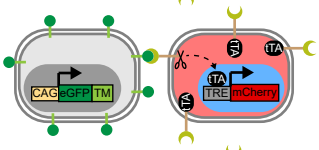

STC receivers + CmGP1 senders

G

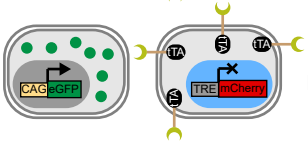

STC receivers + E14GIP1 "senders"

H

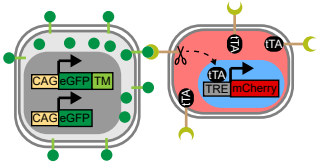

STC receivers + CmGP1GH1 senders

Flow analysis of tagBFP+ GFP- cells

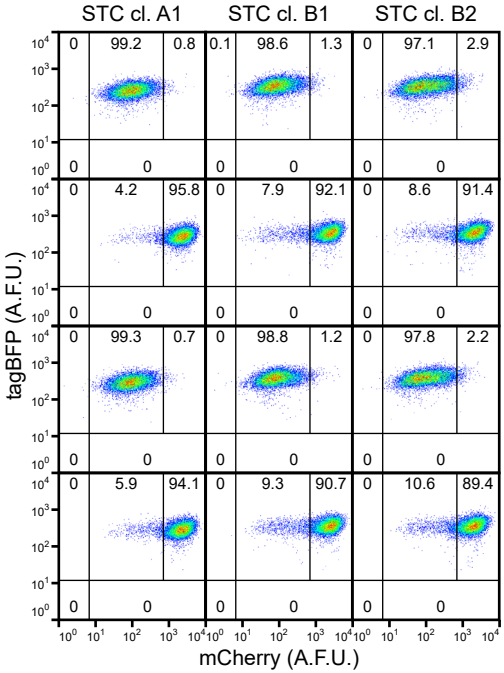

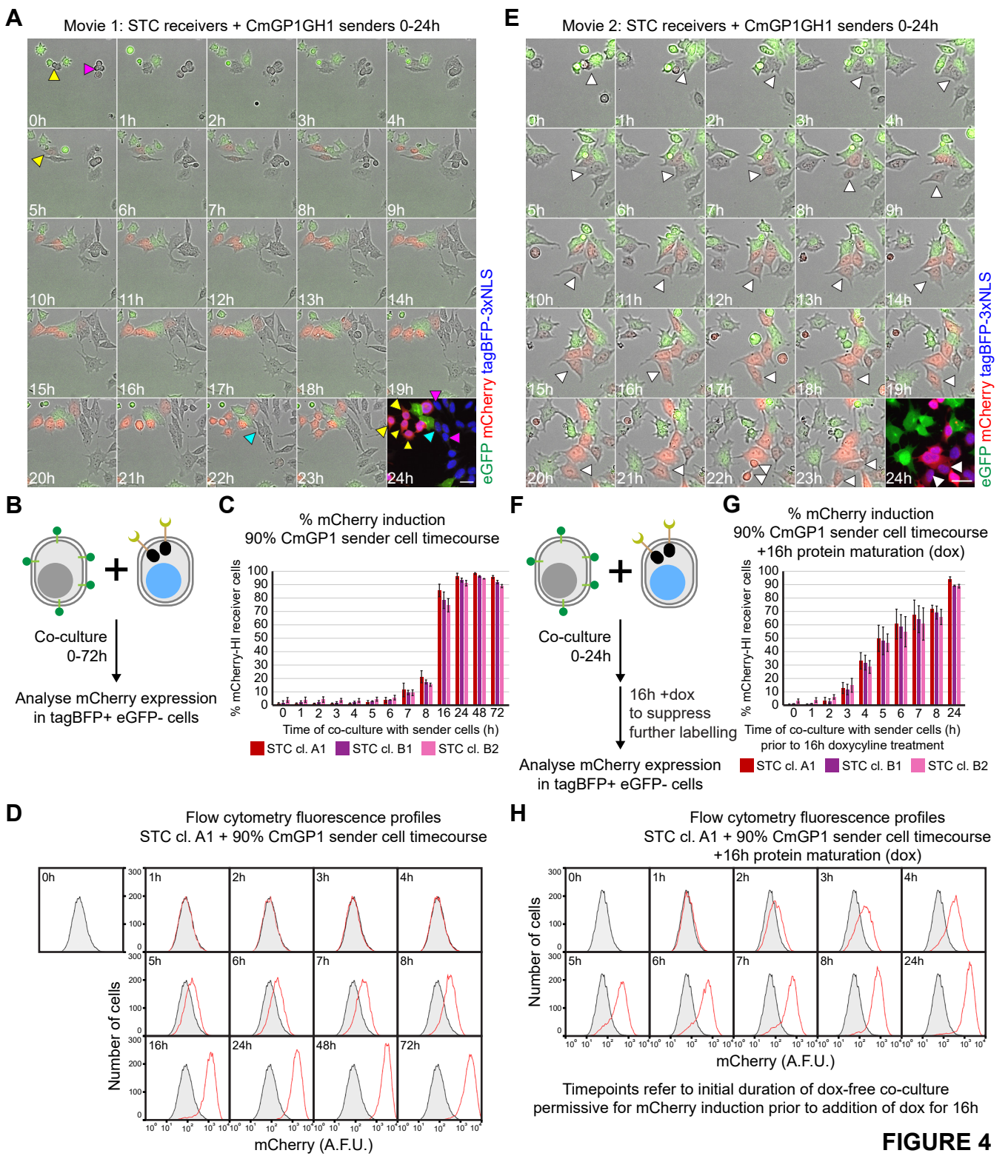
A
Movie 1: STC receivers + CmGP1GH1 senders 0-24h
0h
1h
2h
3h
4h
5h
6h
7h
8h
9h
10h
11h
12h
13h
14h
15h
16h
17h
18h
19h
20h
21h
22h
23h
24h
eGFP mCherry tagBFP-3xNLS
E
Movie 2: STC receivers + CmGP1GH1 senders 0-24h
B
Co-culture
0-72h
Analyse mCherry expression
in tagBFP+ eGFP- cells
C
% mCherry induction
90% CmGP1 sender cell timecourse
% mCherry-HI receiver cells
Time of co-culture with sender cells (h)
STC cl. A1
STC cl. B1
STC cl. B2
F
Co-culture
0-24h
16h +dox
to suppress
further labelling
Analyse mCherry expression
in tagBFP+ eGFP- cells
G
% mCherry induction
90% CmGP1 sender cell timecourse
+16h protein maturation (dox)
% mCherry-HI receiver cells
Time of co-culture with sender cells (h)
prior to 16h doxycyline treatment
STC cl. A1
STC cl. B1
STC cl. B2
D
Flow cytometry fluorescence profiles
STC cl. A1 + 90% CmGP1 sender cell timecourse
Number of cells
mCherry (A.F.U.)
H
Flow cytometry fluorescence profiles
STC cl. A1 + 90% CmGP1 sender cell timecourse
+16h protein maturation (dox)
Number of cells
mCherry (A.F.U.)
Timepoints refer to initial duration of dox-free co-culture
permissive for mCherry induction prior to addition of dox for 16h

FIGURE 4

FIGURE 5

A

Chimaeric blastocysts with STC receiver + CmGP1GH1 sender cells

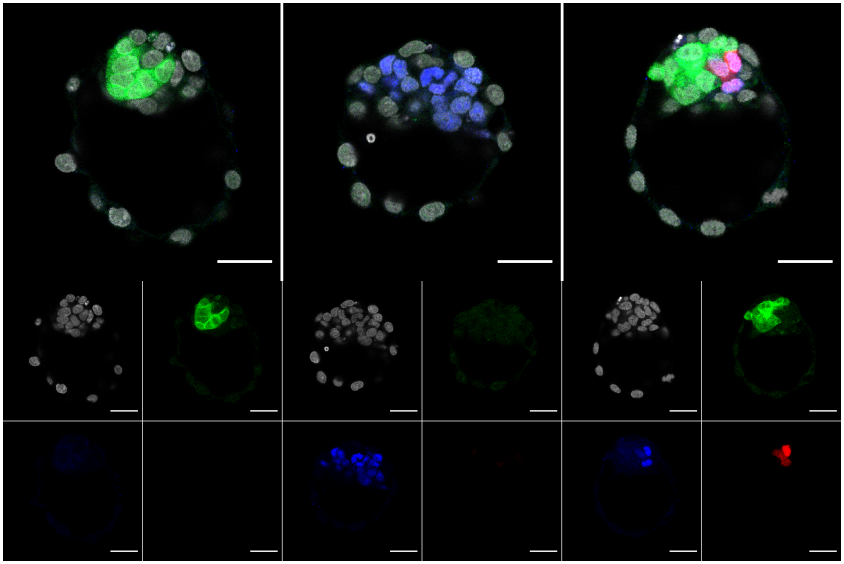

Nuclei eGFP tagBFP-3xNLS mCherry

B

	mCherry-HI embryos / total embryos			
	All clones	STC cl. A1	STC cl. B1	STC cl. B2
Wild-type	**0/6**	-	-	-
Senders only	**0/5**	-	-	-
Receivers only	**1/13**	1/7	0/3	0/3
Receivers+senders	**55/55**	21/21	23/23	11/11

FIGURE 6

A

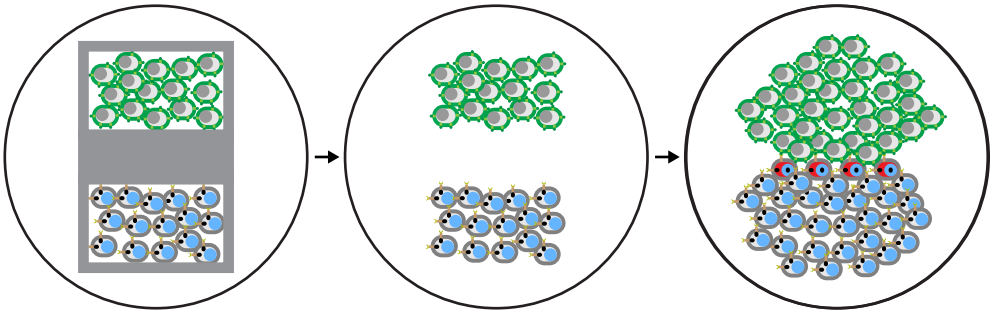

Plate sender and receiver cells in separate wells of multiwell insert

Remove multiwell insert
Give cells time to proliferate

Transgene expression induced at linear interface between sender and receiver cells

B

mCherry induction in STC receivers at sender-receiver border

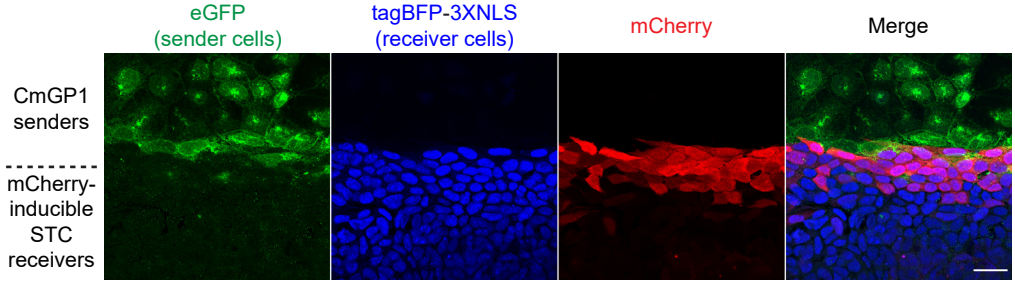

C

STN receiver cells (Neurog1-inducible)

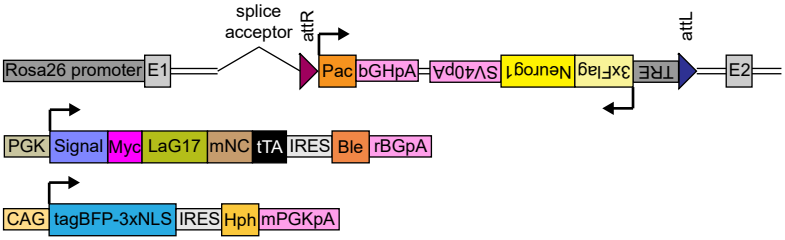

D
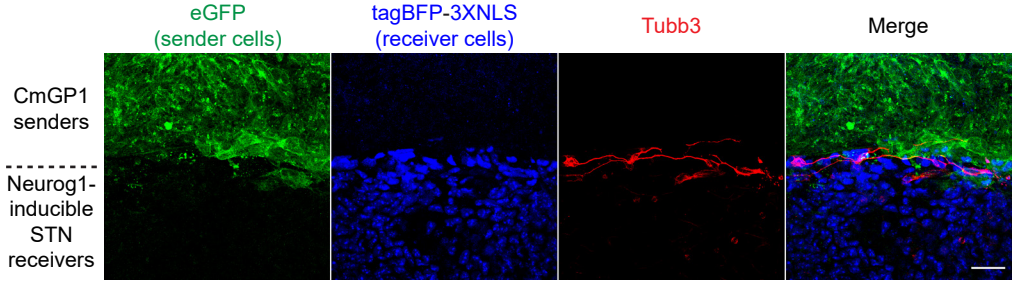
Forced neuronal differentiation of STN receivers at sender-receiver border